Saccharomyces cerevisiae Rev7 regulates DSB repair pathway choice through binding and blocking Mre11 nuclease and Rad50 ATPase activities

Sugith Badugu,[1] Kshitiza M. Dhyani,[1] Manoj Thakur[2] and Kalappa Muniyappa[1*]

[1]Department of Biochemistry, Indian Institute of Science, Bengaluru 560012, [2]Sri Venkateswara College-University of Delhi, New Delhi 110021, India

[*]Corresponding author: E-mail: kmbc@iisc.ac.in; Tel.: +91 80 2293 2235

manoj thakur <manojthakur@svc.ac.in>

IMPACT STATEMENT

The mechanisms steering DNA double-strand break repair pathway choice is a topic of great interest. The present research suggests that yeast Rev7 facilitates non-homologous end-joining by antagonizing homologous recombination.

ABSTRACT

Recent studies in cancer cell lines have shown that the tetrameric Shieldin complex (comprising REV7, SHLD1, SHLD2, and SHLD3) facilitates non-homologous end-joining (NHEJ), while blocking homologous recombination (HR). Surprisingly, several eukaryotic species lack SHLD1, SHLD2 and SHLD3 orthologs, suggesting that Rev7 may leverage an alternative mechanism to regulate the double-strand break (DSB) repair pathway choice. Exploring this hypothesis, we discovered that *Saccharomyces cerevisiae* Rev7 robustly interacts with the Mre11-Rad50-Xrs2 (MRX) subunits, impedes G-quadruplex DNA synergised, HU-induced toxicity and facilitates NHEJ, while antagonizing HR. We identified a 42-aminoacid C-terminal fragment of Rev7 that was critical for its binding to the subunits of MRX complex, protect *rev7Δ* cells from G-quadruplex DNA-HU-induced toxicity and promote NHEJ by inhibiting HR, whereas the N-terminal HORMA domain, a conserved protein–protein interaction module, was dispensable. We further demonstrate that the full-length Rev7 impedes Mre11 nuclease and Rad50's ATPase activities, without affecting the latter's ATP-binding ability. Notably, we found that Rev7 binds with high affinity and specificity to G-

quadruplex structures, as opposed to no binding to mixed-sequence single- and double-stranded DNA. These data uncover unanticipated insights into the functional interaction between the MRX subunits and Rev7, and highlight a mechanism by which it regulates the DSB repair pathway choice between HR and NHEJ in *S. cerevisiae*.

INTRODUCTION

A hallmark of low fidelity DNA polymerases, also known as DNA translesion synthesis polymerases (TLS polymerases), with no detectable proofreading activity, is their ability to catalyse DNA synthesis across a variety of bulky, helix-distorting DNA lesions (Prakash et al., 2005; Vaisman et al., 2017; Maiorano et al., 2021; Ling et al., 2022). As a result, the TLS polymerases play important roles in a plethora of cellular processes, including but not limited to epigenetics, immune signalling, viral mutagenesis and cancer development (Paniagua and Jacobs, 2023). Indeed, translesion synthesis is a source of mutagenesis, potentially contributing to the development of cancer and drug resistance (Lange et al., 2011; Baranovskiy et al., 2012; Pilzecker et al., 2019). The *Saccharomyces cerevisiae* TLS Polζ (hereafter referred to as ScPolζ), comprising catalytic subunit Rev3, two copies of Rev7 regulatory subunits and accessory subunits Pol31 and Pol32, plays a pivotal role in TLS (Johnson et al., 2012; Makarova et al., 2012). Several lines of evidence suggest that the error rate during ScPolζ-catalysed replication of undamaged DNA templates is much higher than that of DNA polymerases, as it lacks 3′-to-5′ proofreading exonuclease activity (Lawrence et al., 1985; Huang et al., 2002; Northam et al., 2006; Zhong et al., 2006; Kochenova et al., 2017). Consistent with this, *S. cerevisiae rev3, rev7* or *pol32* mutant strains show greatly reduced spontaneous mutation frequencies, confirming that ScPol*ζ* is responsible for DNA damage-induced mutagenesis (Quah et al., 1980; Lawrence et al., 1985; Morrison et al., 1989; Nelson et al., 1996, Makarova et al., 2015).

The TLS Polζ is conserved in a wide range of unicellular and multicellular eukaryotes, including fungi, plants, and animals (Maiorano et al., 2021; Ling et al., 2022; Paniagua et al., 2023). While the catalytic subunit Rev3 alone is capable of replicating damaged DNA, Rev7 augments its catalytic efficiency by twenty- to thirtyfold (Quah et al., 1980; Morrison et al., 1989; Nelson et al., 1996, Makarova et al., 2015) and the accessory

subunits Pol31 and Pol32 further raise it by three- to tenfold (Johnson et al., 2012; Makarova et al., 2012), suggesting that they enhance the processivity of translesion DNA synthesis by Polζ (Acharya et al., 2006; Bezalel-Buch et al., 2020). Biochemical and structural analyses have demonstrated that Rev7 (also known as MAD2B and MAD2L2) serves as a bridge between Rev3 and the scaffold protein Rev1 (Haracska et al., 2001; Kikuchi et al., 2012; et al., 2012; Pustovalova et al., 2012). Structural analysis of ScPolζ, using cryo-electron microscopy (cryo-EM), has revealed a remarkable level of organization, wherein its subunits interact with each other and align themselves to form a functional complex (Gómez-Llorente et al., 2013; Malik et al., 2020; Du Truong et al., 2021). Notably, structural studies on the ScPolζ holoenzyme suggest a model wherein subunits Rev3, Rev7, Pol31, and Pol32 form a pentameric ring-shaped structure, facilitated by an uninterrupted chain of protein-protein interaction networks (Gómez-Llorente et al., 2013; Malik et al., 2020; Du Truong et al., 2021). Furthermore, the cryo-EM structure of ScPolζ holoenzyme bound to an A:C mismatch show how the active site pocket accommodates mismatched duplex DNA (Malik et al., 2022).

A deluge of new findings have established that the tetrameric Shieldin complex - comprised of REV7, SHLD1, SHLD2 and SHLD3 – binds single-stranded DNA (ssDNA), blocks 5′ end resection and homologous recombination (HR), antagonizes the recruitment of BRCA1 to the DSB, while facilitating non-homologous end-joining (NHEJ) repair (Xu et al., 2015; Boersma et al., 2015; Mirman et al., 2018; Findlay et al., 2018; Gupta et el., 2018; Ghezraoui et al., 2018; Dev et al., 2018; Tomida et al., 2018; Gao et al., 2018; Noordermeer et al., 2018; Liang et al., 2020). Subsequent studies have demonstrated that the C-terminal “seat belt” region of human Rev7 binds to the N-terminus of SHLD3 (Gupta et el., 2018; Ghezraoui et al., 2018; Dev et al., 2018; Tomida et al., 2018; Gao et al., 2018; Noordermeer et al., 2018; Liang et al., 2020; Clairmont et al., 2020; Dai et al., 2020). Parenthetically, Rev7 deficiency has been linked to disease pathology: a notable example is the Fanconi anaemia in which biallelic *REV7* mutations are associated with hypersensitivity to ICL-forming compounds, accumulation of chromosome breaks during S/G2 phase of the cell cycle and enhanced p53/p21 activation (Bluteau et al., 2016). While Rev7 is most well known as a component of TLS Polζ, it is also involved in the regulation of cell cycle progression by binding to CDH1, an activator of APC/C, modulate the metaphase-to-

anaphase transition and facilitate mitotic spindle assembly and chromosome segregation (Listovsky and Sale, 2013; Vaisman et al., 2017; Ling et al., 2022). However, a mechanistic understanding of how Rev7 regulates cell cycle events and how such roles differ or relate to its role in TLS remains underexplored. Although the emphasis of the findings differs, the fact that Rev7 functions as an anti-resection factor has spurred a new wave of experiments on DNA repair pathways (Setiaputra and Durocher, 2019; Clairmont and D'Andrea, 2021).

At DSBs in *S. cerevisiae*, the Mre11–Rad50-Xrs2 (MRX) in conjunction with Sae2 first catalyses endonucleolytic cleavage of 5′-terminated DNA strands and then its 3'→5' exonucleolytic activity produces a short 3'-ssDNA overhang; subsequently, Exo1 and Dna2-Sgs1 redundantly generate long tracks of ssDNA that are critically important for HR (Cejka and Symington, 2021). As such, the mechanism by which cells restrain over-resection of DSBs is unclear, although hyper-resection could potentially hinder optimal HR and trigger genomic instability. Surprisingly, however, Shieldin orthologs are absent in organisms such as yeast, fruit fly, nematode worm, zebrafish and frog (Setiaputra and Durocher, 2019). These data together prompted us to hypothesize that *S. cerevisiae* Rev7 (hereafter referred to as ScRev7) may recruit an unknown functional equivalent(s) of Shieldin orthologs to regulate the DSB repair pathway choice between HR and NHEJ. We thus reasoned that one specific alternative worthy of consideration is the MRX complex on the basis of current knowledge about its multiple roles in signalling, processing and repair of DSBs (Cejka and Symington, 2021). Here, we provide several lines of evidence, suggesting that ScRev7, through a 42-aminoacid C-terminal fragment in the “safety belt” region, directly interacts with Mre11, Rad50 or Xrs2 subunits, protects *rev7Δ* cells from G-quadruplex DNA/HU-induced toxicity and facilitates efficient NHEJ while antagonizing HR. Mechanistically, ScRev7 binds with low-nanomolar affinity and specificity to G-quadruplex DNA, inhibits Mre11 nuclease and Rad50’s ATPase activities, without affecting the ability of the latter to bind ATP. Collectively, our findings not only reveal unanticipated functional interactions between Rev7 and the MRX subunits, but also provide novel insights into how Rev7 regulates the pathway choice between HR and NHEJ in *S. cerevisiae.*

RESULTS

ScRev7 directly interacts with the MRX subunits

As noted above, studies in cancer cell lines have documented that the Rev7-Shieldin effector complex facilitates NHEJ by blocking 5′ end resection and HR (Xu et al., 2015; Boersma et al., 2015; Mirman et al., 2018; Findlay et al., 2018; Gupta et el., 2018; Ghezraoui et al., 2018; Setiaputra and Durocher, 2019; Cejka and Symington, 2021). Given that Shieldin orthologues are absent *in S. cerevisiae* (Setiaputra and Durocher, 2019), we hypothesized that Rev7 may recruit alternative factors such as the MRX heterotrimer, to block HR and enable NHEJ. To test this premise, yeast two-hybrid assays (Y2H) were performed to identify potential protein–protein interactions between ScRev7 and the M/R/X subunits, whereas in follow-up studies we mapped the minimal region of ScRev7 required for its interaction with the MRX subunits. The yeast strain PJ69-4A was co-transformed with plasmids (prey vectors) encoding the Mre11, Rad50 or Xrs2 subunits and ScRev7 fused to the GAL4 DNA-binding domain (bait vector). The positive colonies were selected on SC/-Trp-Leu-His dropout medium containing 3-aminotriazole (3-AT) (Fields and Song, 1989; James et al., 1996). The results showed robust growth in the selection medium containing 3-aminotriazole (3-AT), indicating Y2H interactions between ScRev7 and the Mre11, Rad50 and Xrs2 subunits (*Figure 1A*), whereas cells bearing empty vector and a plasmid expressing either Mre11, Rad50 or Xrs2 subunits did not yield any Y2H signals. Conversely, yeast cells transformed with prey and bait vectors expressing Rev7 showed robust growth (*bottom panel of Figure 1A*), indicating that Rev7 forms homodimers (Rizzo et al., 2018), which served as a positive control.

Given that Rev3 has been implicated in HR-mediated DSB repair (Sonoda et al., 2003), we asked whether the MRX subunits interact with ScRev7 in the *rev3*Δ mutant strain. To test this hypothesis, the *S. cerevisiae rev3*Δ strain was co-transformed with a combination of bait (pGBKT7 or pGBKT7-*REV7*) and prey vectors (pGADT7, pGADT7-*REV7*, pGADT7-*MRE11*, pGADT7-*RAD50* or pGADT7-*XRS2*). Interestingly, we observed binary interactions between the subunits of MRX complex and ScRev7 in the *rev3*Δ mutant (*Figure 1B*), indicating that Rev3 is not necessary for the interaction between ScRev7 with the MRX subunits. Analogously ScRev7 showed binary interactions with the subunits of MRX complex in the *mre11Δ rad50Δ xrs2Δ* triple mutant strain (*Figure 1C*), further confirming that their association is independent of endogenous MRX subunits.

ScRev7 exhibits high-affinity binding to the MRX subunits

Microscale thermophoresis (MST) allows for quantitative analysis of protein-protein interactions in free solution (Wienken et al., 2010). Since the binding of ScRev7 to the MRX subunits was unexpected, we sought to validate their interaction by an orthogonal assay and determine their binding affinities using purified proteins. We assessed the binding of ScRev7-eGFP (*Figure 1—figure supplement 1 and 2*) to the Mre11, Rad50 and Xrs2 subunits using the MST assay. The fraction of the indicated protein bound to ScRev7-eGFP was plotted as a function of concentrations (*Figure 1D*). Normalized MST data were fitted to a logistic binding curve, resulting in an apparent dissociation constant (K_d) of 0.16 ± 0.07 and 0.23 ± 0.06 μM for Rad50 and Mre11 subunits, respectively, which is two- to threefold greater compared to Xrs2 (*Figure 1F*). To confirm these findings, we purified *S. cerevisiae* Rev1 (*Figure 1—figure supplement 3*) and assessed its interaction with ScRev7 as positive control. Consistent with previous studies (Rizzo et al., 2018; Guo et al., 2003), our results showed that Rev1 interacts with Rev7 with an affinity similar to that of Rev7 and Rad50 interaction (*Figure 1D* and *F*). On the other hand, our results demonstrated that the MRX subunits do not interact with the negative control eGFP reporter (*Figure 1E*). It is also noteworthy that the Hill coefficients (n_H) indicate larger than one, implying positive cooperativity (*Figure 1F*). The quantitative assessment of binding affinities together with Y2H data suggest that ScRev7 robustly interacts with the MRX subunits.

Models predicted by AlphaFold-Multimer reveal that Mre11 and Rad50 subunits independently associate with Rev7

To further characterize the interaction between the MRX subunits and ScRev7, we used a structure prediction algorithm, AlphaFold-Multimer (Evans et al., 2022), to generate structural models of ScRev7-Mre11 and ScRev7-Rad50 heterodimers. The models with the high pLDDT scores were considered for further analysis. Strikingly, the models indicated that Mre11 and Rad50 binding surfaces overlap with ScRev7 and thereby suggesting that the latter can only bind one of these proteins at a time (*Figure 1*). In the model of Rev7-Mre11 complex, residues Asp 206 and Ile 240 in the Rev7 C-terminal “safety belt region” (green) mediate dimerization with Mre11 through

residues Asp 131 and Arg 181. Interestingly, His 127 in the Rev7 N-terminal HORMA domain also contribute its binding to Asp 131 of Mre11 (*Figure 1—figure supplement 4A, Supplementary Table S1*). Furthermore, inspection of Rev7-Rad50 complex model showed that the ScRev7 C-terminal residues Lys 168, Glu 184, Asn 189 and Asp 188 mediate dimerization with ScRad50 via residues Glu 577, Lys 596 and Arg 603 (*Figure 1—figure supplement 4B, Supplementary Table S2*). Curiously, AlphaFold-Multimer models also revealed that amino acid residues outside of the 42-residue fragment also contribute to pairwise interactions between Rev7 and the Mre11 and Rad50 subunits, although Y2H assays did not identify such interaction. Indeed, similar findings have been previously noted for several other interacting partners (You et al., 2006; Koegl and Uetz, 2007; Hoff et al., 2010). A structural model of Rev7-Xrs2 heterodimer was not generated because Xrs2 alone has no known biochemical activity and thus was not considered for further investigation.

A 42-aminoacid C- terminal segment of ScRev7 is critical for its interaction with the MRX subunits

As the data from Y2H and MST assays, as well as AlphaFold-Multimer-based structural modelling, implied direct interaction between the MRX subunits and ScRev7, we sought to identify the putative functional domains in the ScRev7 in regulating the function of MRX subunits. To this end, we generated three N-terminally truncated species and an equal number of C-terminally truncated variants. We refer to these variants as Rev7-N1; Rev7-N2; Rev7-N3, and Rev7-C1, Rev7-C2 and Rev7-C3, respectively (*Figure 2A*). We then examined for their ability to associate with the MRX subunits and thus survival of yeast cells on selective medium. Our experiments surprisingly revealed that cells expressing the ScRev7 N-terminally truncated variants showed robust growth in selection medium (*bottom panel of Figure 2B*) similar to the WT (*Figure 1A-C*), indicating that they associate with the subunits of MRX complex. Further, these results also revealed that the HORMA domain encompassing residues 1-149 at the N-terminus, an evolutionarily conserved protein–protein interaction module, is dispensable for interaction between the MRX subunits and ScRev7 (*Figure 2B*). Notwithstanding, we cannot exclude the possibility that it may play a function that is undetectable by the Y2H assay. We then performed Y2H experiments using the C-terminally truncated species (*Figure 2C*). Notably, deletion of C-terminal 42-amino

acid residues (i.e., 203-245) completely abolished the viability of the yeast cells (*bottom panel of Figure 2C*). Similar abrogation of cell viability was also caused by deletion of the C-terminal 150 to 203 amino acid residues of ScRev7 (*Figure 2C*). These results indicate that the C-terminal 42-residue segment of ScRev7 is critical for interaction with the MRX subunits.

However, it remained possible that the inability of cells expressing the C-terminally truncated variants of ScRev7 (with appropriate prey proteins) to grow in selection medium (Figure 2C, *bottom panel*) may be due to altered expression or decreased abundance of truncated species. To explore this possibility, whole cell lysates of cells expressing the N- and C-terminally truncated variants, tagged with c-Myc epitope at the N-terminus, were harvested and analysed by immunoblotting using an anti-c-Myc antibody. Reassuringly, similar amounts of N- and C-terminally truncated species of were detected in the whole cell lysates of strains that were employed for Y2H analyses (*Figure 2—figure supplement 1*).

The C-terminal 42-residue fragment of ScRev7 mitigates the G-quadruplex-HU induced toxic effects

Several studies have documented the genome-wide prevalence of G-quadruplex DNA structures in various organisms ranging from viruses to humans, which play regulatory roles in diverse cellular processes (Rhodes and Lipps, 2015; Spiegel et al., 2020; Yadav et al., 2021). For instance, it has been shown that Rev1-deficient chicken DT40 cells exhibit defects in replicating G quadruplex-forming motifs (Sarkies et al., 2010, 2012). Similarly, computational and genetic studies in *S. cerevisiae* have revealed that G-quadruplex-forming motifs cause slow growth in replication stressed Pif1 deficient cells and affect genome integrity (Capra et al., 2010; Paeschke et al., 2011, 2013). Inspired by these findings, we asked whether ScRev7 plays a role in genome maintenance using the assay developed by the V. Zakian lab (Paeschke et al., 2011). To investigate these questions, we first assessed the growth of WT and *rev7*Δ mutant cells under normal growth conditions and under conditions of HU-induced replication stress in the absence of G-quadruplex forming sequences. This analysis

revealed that, like the WT, *rev7*Δ mutant cells grew robustly in the absence or presence of HU (*Figure 3A*).

Next, we asked whether the G-quadruplex DNA motifs affect cell viability in the absence or presence of DNA damaging agents, such as HU. To this aim, we tested the effect of G-quadruplex forming sequences, positioned on either the leading or lagging template strands, on the growth of WT, *rev7*Δ mutant and cells expressing the ScRev7 variants (Rev7-C1 or 42-residue C-terminal segment) in the absence or presence of HU. We found that all the tested strains showed robust growth in the absence of HU (*Figure 3B*). On the other hand, while HU had no effect on the growth of WT cells, *rev7*Δ mutant was extremely sensitive to HU and this was also the case with cells expressing the variant Rev7-C1 (*Figure 3C*). Gratifyingly, however, cells expressing the 42-residue C-terminal segment of Rev7 exhibited robust growth as the WT in the presence of HU (*Figure 3C*). These results suggest that the 42-residue C-terminal segment, but not Rev7-C1 variant, can protect cells from the toxic effects of HU and G-quadruplex DNA forming sequences, regardless of whether they are in the leading or lagging template strands.

Rev7 exhibits high-affinity for G-quadruplex DNA structures

Despite extensive cellular and structural characterization of ScRev7 (Setiaputra and Durocher, 2019; Clairmont and D'Andrea, 2021), it is unknown whether it can recognize and bind to specific DNA sequences or has any enzymatic activity. In this regard, our results revealed that *REV7* alleviates G-quadruplex DNA synergised, HU-induced toxicity, raising the possibility that ScRev7 may interact with G-quadruplex DNA structures. To test this premise, ScRev7 and ScRev7-C1 were expressed in and purified from *E. coli* whole cell lysates to homogeneity (*Figure 4A* and *4B*). Electrophoretic mobility shift assays (EMSA) were performed under physiological conditions to test for their ability to bind a suite of ^{32}P-labeled DNA substrates. In a protein titration experiment, we found that ScRev7 bound effectively to the G-quadruplex DNA substrates (TP-G4, 6G3-G4 and 4G3-G4), yielding >90% protein-DNA complexes at the protein concentrations used (*Figure 4C —figure supplement 1A-C*). By contrast, it exhibited no detectable binding to mixed-sequence ssDNA or dsDNA (*Figure 4— figure supplement 1D-E*). Furthermore, the mobility of ScRev7-

DNA complexes was progressively decreased with increasing ScRev7 concentrations, suggesting cooperative binding of ScRev7 to G-quadruplex structures. As expected, the binding was lost when the G4 DNA capable sequences were mutated (*Figure 4C* and *4D –figure supplement 1F*). Based on the bound and the unbound DNA from multiple EMSA experiments, the apparent binding affinities (K_d) of ScRev7 for various G4 DNA substrates was determined and found to be in the low nanomolar range (*Figures 4B* and *4C*). Under identical conditions, ScRev7-C1 variant showed no detectable binding to G4 DNA (*Figure 4—figure supplement 1G*). Interestingly, we observed that the affinity (K_d) of ScRev7 increases with increasing number of contiguous guanine residues (i.e., TP-G4 > 6G3-G4 > 4G3-G4; *Figure 4D*). The apparent K_d values obtained for ScRev7 are comparable to those reported for several G4 DNA-binding proteins using similar substrates (Rhodes and Lipps, 2015; Spiegel et al., 2020; Yadav et al., 2021). These results indicate that ScRev7 binds to G-quadruplex structures and thereby might counteract genome instability induced by these structures. Additionally, these data suggest that ScRev7 is a novel G4 DNA-binding protein.

Rev7 inhibits Mre11 nucleolytic activities

From analysis of the history of trimeric MRX complex, it is clear that Mre11 is a bifunctional enzyme that binds dsDNA ends and displays both endo- and exonuclease activities, which are critical for DNA end resection (Ghosal and Muniyappa, 2007; Ghodke and Muniyappa, 2013; Paull and Gellert, 1998; Tsubouchi and Ogawa, 1998; Stracker and Petrini, 2011; Paull, 2018; Casari et al., 2019). Further, it has been demonstrated that Mre11 cleaves non-B DNA structures such as DNA hairpins, cruciforms and intra- and inter-molecular G-quadruplex structures (Ghosal and Muniyappa, 2007; Trujillo and Sung, 2001; Lobachev et al., 2002; Ghosal and Muniyappa, 2005). To explore the functional significance of Mre11-Rev7 complex formation, an assay was performed wherein 5'-^{32}P-labelled dsDNA and MRX subunits (in equimolar amounts) were incubated in the absence or presence of ScRev7. The reaction products were analyzed as previously described (Ghosal and Muniyappa, 2005). The results informed that: (a) ScRev7 has no nuclease activity (*Figure 5A, lane 2*) and (b) Mre11 cleaved ^{32}P-labelled dsDNA, resulting in a ladder-like pattern of DNA products (*Figure 5A, lane 3*). We then examined the effect of ScRev7 on MRX

nuclease activity by co-incubating various concentrations of ScRev7 and fixed amounts of MRX subunits, prior to the addition of 5'-^{32}P-labelled dsDNA. The results revealed that ScRev7 inhibited the MRX cleavage activity in a dose-dependent manner and almost complete inhibition was observed at 2 μM (*Figure 5A, lanes 4-12*). Interestingly, somewhat similar results were obtained with ScRev7-C1, although its inhibitory effect was noticeably less efficient than that of full-length ScRev7. Based on these data, we surmise that ScRev7-C1 does not faithfully recapitulate the Y2H results. Although the reason for this remains unclear, one possible reason for these discrepant results might be due to the interaction of amino acid residues in the ScRev7-C1 with Mre11, consistent with AlphaFold-Multimer modeling of the ScRev7-Mre11 heterodimer structure.

Many studies have demonstrated that Mre11 exhibits both endonuclease and exonuclease activities independently of Rad50 and Xrs2 subunits (Cejka and Symington, 2021). Thus, we next examined the effect of ScRev7 on the Mre11 ssDNA-specific endonuclease activity in reactions lacking Rad50 and Xrs2. Consistent with previous reports, we observed Mre11 digested all the input substrate into small fragments/nucleotides in a manner dependent on its concentration (*Figure 5C*). Interestingly, we found that the addition of increasing concentrations of ScRev7 coincided with a concomitant decrease in the Mre11 endonuclease activity (*Figure 5D*), although it retained ssDNA nicking activity generating liner ssDNA. Together, these results support the idea that inhibition of Mre11 endonuclease activity is due to its direct interaction with ScRev7, as the latter is devoid of ssDNA and dsDNA binding activities (*Figure 4*).

ScRev7 impedes Rad50's ATPase activity without affecting its ATP binding ability

Several studies have demonstrated that the ATPase activity of Rad50 plays an important regulatory role in DNA recombination/repair functions (Cejka and Symington, 2021). Intrigued by the direct interaction of ScRev7 with ScMre11 and Rad50 subunits, we asked whether ScRev7 affects the ability of Rad50 to bind ATP and catalyze its hydrolysis. To test this possibility, different concentrations of

purified Rad50 were incubated with [γ-^{32}P]ATP. Because this interaction is transient, the reaction mixtures were irradiated with UV light prior to subjecting the samples to SDS/PAGE. In this analysis, we found a single band that migrated as a 153 kDa species, which corresponds to the molecular mass of ScRad50 (*Figure 6A*). Quantitative analyses indicated that Rad50 binds [γ-^{32}P]ATP in a concentration dependent manner (*Figure 6B*). Parallel experiments uncovered no significant differences in the extent of [γ-^{32}P]ATP bound by Rad50 in the presence or absence of ScRev7 (*Figure 6C*). This finding suggests that ScRev7 does not affect the ability of Rad50 to bind ATP (*Figure 6D*).

We next evaluated whether ScRev7 affects the ability of Rad50 to catalyze ATP hydrolysis using thin layer chromatography coupled with an image analysis. Consistent with previous work (Ghosal and Muniyappa, 2007), control reactions showed that Rad50 catalyzed [γ-^{32}P]ATP hydrolysis to ADP and ^{32}Pi, which increased in a manner dependent on its concentration (*Figures 6E* and *F*). Interestingly, while ScRev7 itself has no ATPase activity, it suppressed ATP hydrolysis of Rad50 in a dose-dependent manner (*Figures 6G* and *I*). Similar analysis showed that the ScRev7-C1 blocked ATP hydrolysis by Rad50, although three-fold less efficiently compared with full-length ScRev7 (*Figures 6H* and *I*). As noted above, a possible explanation for this observation is that amino acid residues in the ScRev7-C1 may interact with Rad50, consistent with AlphaFold-Multimer modeling of the ScRev7-Rad50 heterodimer structure. These results were validated using colorimetric molybdate/malachite green-based assay (Lanzetta et al., 1979). While ScRev7 blocked approximately 60% of total ATPase activity of Rad50 at the highest dose tested, Rev7-C1 exerted partial inhibitory effect in the same range of concentrations (*Figure 6—figure supplement 1*). Collectively, these data support a model wherein the effect of ScRev7 extends beyond being a passive binder of MRX subunits, but negatively affects their catalytic activities.

REV7* facilitates NHEJ in *S. cerevisiae

In *S. cerevisiae*, the heterotrimeric MRX complex has been implicated in both Ku-dependent NHEJ and microhomology-mediated end joining repair (Zhang and Paull, 2005; Boulton and Jackson, 1998; Moore and Haber, 1996; Ma et al., 2003). Multiple

studies in cancer cell lines have shown that Rev7 inhibits DNA end-resection and favors NHEJ over HR (Gupta et el., 2018; Ghezraoui et al., 2018; Dev et al., 2018; Gao et al., 2018; Liang et al., 1972). To our knowledge, it is unknown whether these findings have been extended to other species. However, *Schizosaccharomyces pombe* Rev7 has been shown to inhibit long-range resection at DSBs (Leland et al., 2018). Furthermore, it is unclear whether the *S. cerevisiae* Rev1, Rev3 and Rev7 subunits are required for NHEJ. To investigate this, the efficiency of plasmid-based NHEJ repair was analyzed by transforming BamHI-linearized plasmid pRS416*,* which has no homology with the genomic DNA, into the WT and isogenic mutant strains as described (Boulton and Jackson, 1998; Moreau et al., 1999) (*Figure 7A*). Consistent with a previous study (Boulton and Jackson, 1998), we observed that NHEJ was undetectable in the *mre11⊿* mutant (*Figure 7B, Supplementary Table S3*). Notably, while the *rev1Δ and rev3*Δ strains showed a modest decrease in the efficiency of NHEJ, *rev7Δ* single and *rev1Δ rev3*Δ double mutants exhibited approximately four- and twofold decrease, respectively, compared with the WT. Further analysis revealed that the NHEJ efficiency in double mutants - *rev1Δ rev7Δ, rev3*Δ *rev7Δ* and *sae2Δ rev7Δ* - was comparable to that of *rev7Δ* mutant (*Figure 7B* and *7C* —*Supplementary Table S3*). Intriguingly, however, we found that ScRev7-42 aa peptide, but not the Rev7-C1 variant, fully restored NHEJ efficiency in *rev7Δ* cells to the WT levels. Together, these data indicate that Rev7 augments the efficiency to NHEJ-mediated DSB repair in *S. cerevisiae*.

Next, we sought to verify our plasmid-based NHEJ results in a chromosomal context. To this aim, the NHEJ efficiency was determined using “suicide-deletion” assay in which the I-SceI induced DSB may be repaired preferentially via NHEJ (Karathanasis and Wilson, 2002). Briefly, it is based on an approach wherein galactose-induced I-SceI endonuclease creates a pair of site-specific DSBs, resulting in the deletion of its own coding region, thereby facilitating NHEJ-mediated repair (*Figure 8A*). Using this approach, we determined the frequency of Ade2+ recombinants in the WT and isogenic mutant strains. A critical NHEJ factor Ku70 was used as a control. As expected, while NHEJ was undetectable in strains lacking *MRE11* and *KU70*, deletion of *REV7, REV1* and *REV3* led to a 9-fold, 2.3-fold- and 3.2-fold decrease, respectively, in the frequency of NHEJ compared with the WT. Of note, a

fourteen-fold decrease in the frequency of Ade2+ recombinants were observed in the *rev7-C1* cells, which could be restored to WT levels by expressing the C-terminal 42 amino acid peptide (*Figure 8B, Supplementary Table S4*). The results reinforce the notion Rev7 promotes NHEJ repair at DSBs. The PCR product derived from genomic DNA of Ade2+ recombinants showed a 1.3 kb amplicon, suggesting faithful repair of I-SceI induced DSB (*Figure 8C*).

REV7* suppresses HR in *S. cerevisiae

As noted above, the RIF1/REV7/Shieldin complex blocks DNA end resection and BRCA1-mediated HR, but promotes DSB repair through NHEJ in cancer cell lines (Gómez-Llorente et al., 2013; Malik et al., 2020; Du Truong et al., 2021; Xu et al., 2015; Boersma et al., 2015; Mirman et al., 2018; Findlay et al., 2018; Gupta et el., 2018; Ghezraoui et al., 2018; Dev et al., 2018; Tomida et al., 2018; Gao et al., 2018; Noordermeer et al., 2018; Liang et al., 2020); however, the generality of this finding remained largely uncharacterized. To this end, we leveraged a spot assay (Paeschke et al., 2013) to assess the putative role of *S. cerevisiae REV7* in HR. In this assay, we examined the recombination frequency, under replication stress and standard growth conditions, between the *ura3-1* allele located at its endogenous location on chromosome V and *ura3-G4* allele on the pFAT10-G4 plasmid (*ura3* allele interrupted by G4 motifs) (*Figure 9A*). While Ura3$^+$ papillae formation was not observed in the *ura3-1* strain carrying the empty vector in both selective and non-selective media, the same strain with a plasmid containing G-quadruplex capable sequences exhibited Ura3$^+$ papillae formation, albeit fewer, only under non-selection conditions. Of note, we found that the *ura3-1 rev7*Δ strain carrying a plasmid with G-quadruplex motifs displayed a significant number of Ura3$^+$ papillae on non-selective and selective media, indicating that *REV7* suppresses HR frequency (*Figure 9B*). Consistent with a previous report (Cejka and Symington, 2021), the nuclease-deficient mutant *mre11-D56N,H125N* alone (used as a positive control) and in combination with *rev7*Δ had no discernible effect on Ura3+ papillae formation on selective medium (*Figure 9B*). As expected, neither ScRev7-42 residue peptide nor Rev7-C1 altered the frequency of Ura3+ papillae formation on selective medium (*Figure 9B, bottom two rows*). Quantification revealed that the *ura3-1 rev7*Δ double mutant showed a 2.4-fold increase in HR frequency as compared to *ura3-1* and

ura3-1 mre11-D56N,H125N mutant strains (*Figure 9C*). Since all tested strains formed Ura+ papillae in the absence of HU approximately at a similar frequency, they are likely to arise due to spontaneous DSBs and collapsed replication forks.

To confirm whether the G-quadruplex motifs stimulate HR in the *rev7Δ* strain, the frequency of HR was determined using pFAT10-G4 -mut plasmid with mutated G4 sequences. The results revealed that the rate of HR frequency decreased by 5.8-fold compared to strain carrying plasmid pFAT10-G4 -mut with unmutated sequences, indicating that this decrease is due to mutation of G-quadruplex–forming sequences (*Figure 9—figure supplement 1*). To assess whether increased frequency of HR is due to the instability of G-quadruplex DNA in *rev7Δ* cells, we examined the length of G4 DNA inserts in the plasmids carrying sequences during HR assay. We found a DNA fragment of approximately 829 bp corresponding to the expected size in both WT and *rev7Δ* cells (*Figure 9—figure supplement 2*). It is therefore possible that increased frequency of HR in *rev7Δ* cells could be due to the loss of Rev7 function rather than instability G4 DNA capable sequences. Viewed together, these findings are consistent with the idea that *REV7* completely abolishes DSB-induced HR in *S. cerevisiae*.

DISCUSSION

In this study, genetic and biochemical analyses of the wild-type ScRev7 and its 42 residue variant have revealed unanticipated insights into the mechanism by which Rev7 regulates the DSB repair pathway choice between HR and NHEJ in *S. cerevisiae.* Specifically, we show that ScRev7 directly interacts with the individual subunits of the MRX complex via a 42-residue C-terminal fragment (residues 203-245), protects cells form G4 DNA-HU induced toxicity, facilitates NHEJ while blocking HR, thereby suggesting that this minimal region harbors structural principles required for Rev7 function *in vivo*. Additionally, we found that ScRev7 impedes Mre11 nuclease and Rad50's ATPase activities, without affecting the latter's ATP-binding capacity. We further show that ScRev7 binds with significantly high affinity (K_d in the range of 3.22 to 18.26 nM) to G-quadruplex structures, as opposed to no binding to mixed-sequence ssDNA and dsDNA. When seen from a teleological perspective, these findings are conceptually reminiscent of Shieldin complex-mediated suppression of 5′ end resection and repair of DSBs via NHEJ

while antagonizing HR in cancer cell lines (Xu et al., 2015; Boersma et al., 2015). At this stage, we tentatively speculate that this alternative mechanism of regulation of DSB repair pathway choice in *S. cerevisiae* may be conserved across multiple species.

Historically, *REV7* was discovered as playing an important role in DNA damage-induced mutagenesis in *S. cerevisiae* (Lemontt, 1971; Lawrence and Das, 1985). Further analyses showed that Rev7 associates with Rev3 and functions as a regulatory subunit of eukaryotic TLS DNA polymerase Polζ (Prakash et al., 2005; Maiorano et al., 2021; Ling et al., 2022; Paniagua and Jacobs, 2023). Of note, Rev7 has no known catalytic activity, but serves as a versatile scaffolding protein: the versatility of Rev7 is underpinned by its unique ability to function in diverse cellular processes, including TLS, DNA repair and cell cycle that were initially considered inconceivable (de Krijger et al., 2021; Decottignies, 2013). However, little is known about the nature of specific effector(s) that associate with Rev7 and regulate DSB repair in *S. cerevisiae.* As we discuss below, the Y2H assays showed unequivocally that ScRev7 interacts with the individual subunits of MRX complex. Consistent with this, MST analysis and AlphaFold-Multimer models revealed tight association between the MRX subunits and ScRev7. On the other hand, while co-immunoprecipitation experiments implicated that Mre11, Rad50 and Xrs2 subunits exist as a hetero-trimeric complex *in vivo* (Usui et al., 1998), *in vitro* experiments have shown the formation of dimeric Mre11-Rad50 and trimeric MRX complexes (Oh et al., 2016; Arora et al., 2017). Additionally, to our knowledge, the relative amounts of monomeric, dimeric and trimeric species of MRX subunits *in vivo* are unknown. Relatedly, current models suggest that Mre11 and Rad50 bind to DNA in Rad50/Mre11-dependent and -independent manner (Stracker and Petrini, 2011; Paull, 2018; Casari et al., 2019). This leads us to postulate that the monomeric, dimeric and trimeric species of MRX subunits may exist in a dynamic equilibrium under *in vivo* conditions.

Given that Rev7 and MRX subunits play essential roles in DNA repair pathways, our findings provide intriguing insights into how ScRev7 interacts with the MRX subunits. Structure-function analysis showed that deletion of 42-amino acid fragment (203-245) at the extreme C-terminus of ScRev7 abolished its binding to the MRX subunits,

whereas loss of the N-terminal HORMA domain, an evolutionarily conserved protein-protein interaction module (de Krijger et al., 2021; Muniyappa et al., 2014; Rosenberg and Corbett, 2015) had no discernible effect on its interaction. Curiously, further analysis indicated that the 42-residue peptide alone was sufficient for its binding to the MRX subunits and regulation of DSB repair pathway choice between NHEJ and HR. Analogously, it will be of interest to determine the regions/domains of MRX subunits that interact with ScRev7 for a comprehensive understanding of the crosstalk between these components. Work is currently in progress to gather insights into these questions.

The data from MST-based assays informed that ScRev7 binds to MRX subunits with significant affinity, analogous to the interaction between HORMA-domain protein hMAD2 and hCDC20 (Piano et al., 2021). How might ScRev7 suppress the function of Mre11 and Rad50 subunits? Encouraged by the above-mentioned results, we tested the effect of ScRev7 on the biochemical activities of MRX subunits. Reassuringly, we found that nanomolar amounts of ScRev7 besides adversely affecting the Mre11 nuclease activity also impeded Rad50's ATPase activity without obstructing its ability to bind ATP. Whilst the specific nuances of the interaction await further characterization, we surmise that direct association between ScRev7 and the Mre11/Rad50 subunits might contribute to the observed effects. Although we provide compelling *in vivo* evidence that the Rev7 C-terminal 42-residue peptide is critical for binding to the MRX subunits, rescue cells from G4 DNA-HU-induced toxicity and regulate the pathway choice between NHEJ and HR, we could not demonstrate its function *in vitro* because our multiple attempts to express and purify the peptide were unsuccessful. Unexpectedly, however, we found that the Rev7-C1 variant, which lacks the ability to interact with the MRX subunits in Y2H assays, partially blocked the catalytic activities of Mre11 and Rad50 subunits *in vitro*. Why this is the case is not clear, but one possibility is that amino acid residues outside the 42-residue fragment facilitate pairwise interactions between ScRev7 and the Mre11 and Rad50 subunits, as seen in AlphaFold-Multimer models. Conversely, the 42-amino acid fragment as a part of whole protein could potentially block the residues in the Rev7-C1 fragment, thereby enabling it to function effectively as a single site for binding to the MRX subunits in Y2H assays. Future studies are required to test this hypothesis.

Many lines of evidence indicate that G-quadruplex capable sequences are measurably enriched at certain functional regions in the genomes of all organisms, from humans to plants to microbes (Capra et al., 2010; Huppert and Balasubramanian, 2005; Lejault et al., 2021; Castillo Bosch et al., 2014). Furthermore, G-quadruplex structures modulate diverse cellular processes, including DNA replication, transcription, translation, and are associated with certain diseases, characterized by high rates of chromosomal instability (Rhodes and Lipps, 2015; Spiegel et al., 2020). Serendipitously, we found that deletion of *REV7* resulted in G4 DNA-associated genomic instability during DNA replication, rendering cells hypersensitive to HU-induced genotoxic stress and cell death. This is consistent with accumulating evidence that DNA replication stress induced by G-quadruplex structures play a prominent role in triggering genomic instability, which is exacerbated in the presence of HU (Sato and Knipscheer, 2023). To this end, G-quadruplex DNA-specific binding properties of ScRev7 defined here enabled us to provide a possible explanation for its role in protecting cells against G-quadruplex-induced hypersensitivity to HU. Curiously, it was found that Rev7 binds with high affinity to G-quadruplex structures, as opposed to ssDNA or dsDNA containing random sequences. However, we cannot exclude the possibility that additional, less abundant, preferred DNA substrates may exist for Rev7 in *S. cerevisiae* cells. Based on published literature and our studies, it is tempting to speculate that ScRev7 may recruit G4-resolving helicase(s) such as Sgs1 and Pif1 to unwind G-quadruplex structures prior to or during DNA replication (Huber et al., 2002, Paeschke et al., 2013). Alternatively, or in addition, it may generate G4 DNA intermediates which may be processed by specific enzymes such as Mus81 or Sgs1/Top3. Regardless, our data align with the notion that G-quadruplex structures are endogenous sources of replication stress and their formation and persistence may lead to genomic instability and cell death.

Several studies have shown that Shieldin complex facilitates NHEJ-dependent DSB repair, while inhibiting DNA end resection and HR in cancer cell lines (Clairmont and D'Andrea, 2021; Paniagua and Jacobs, 2023). Since 5′ end resection is the primary step in HR-mediated DSB repair, we hypothesized that direct interaction between ScRev7 and MRX subunits might block resection of DNA termini, and then facilitate NHEJ-dependent DSB repair instead of HR. Consistent with this, we found

that ScRev7 augments the efficiency of NHEJ while antagonizing HR. However, other regulatory components may also play a role in modulating the levels of NHEJ versus HR-mediated DSB repair. For instance, TRIP13 or p31^{comet} inhibits the interaction of Rev7 with the SHLD3 subunit and regulates DNA end resection at DSBs and promotes their repair by HR (Sarangi et al., 2020). Additionally, interaction between Rev7 and putative binding partners may be regulated by posttranslational modifications and chromatin accessibility under changing physiological conditions.

Although a comparison of the mechanism of Rev7-mediated regulation of DSB repair between the yeast and cancer cell lines indicate broad similarities, we observed some notable differences. A fundamental difference between the results from cancer cell lines and *S. cerevisiae* is that, while ScRev7 robustly interacts with and suppresses the biochemical activities of both Mre11 and Rad50 subunits to facilitate NHEJ, Rev7-Shieldin complex acts as a downstream effector of 53BP1-RIF1 in restraining DNA end resection to promote NHEJ (Clairmont and D'Andrea, 2021; Paniagua and Jacobs, 2023). Furthermore, hRev7 interacts with the SHLD3 subunit via the HORMA domain, which is entirely dispensable in the case of ScRev7. Interpreted broadly, the highly complex, Shieldin complex-mediated regulation of DSB repair pathway choice might be a source of evolutionary innovation as an additional layer of regulation. In summary, our data bridges a notable gap in the current understanding of the molecular mechanism underpinning ScRev7-mediated regulation of DSB repair pathway choice in *S. cerevisiae.*

MATERIALS AND METHODS

S. cerevisiae strains, DNA plasmids and oligonucleotides

All strains and primers used for the construction of DNA substrates used in this study are listed in Supplementary Table S5 and S6, respectively. The plasmids FT10/Chr.IV$_{G4}$_lg and FT10/Chr.IV$_{G4}$_le were a kind gift from Dr. Virginia Zakian.

Construction of strains used in the study

S. cerevisiae W1588a haploid strains carrying *rev1*Δ, *rev3*Δ, *rev7*Δ , *rev1*Δ *rev3*Δ, *rev1*Δ *rev7*Δ, *rev3*Δ, *rev7*Δ *mre11*Δ or *sae2*Δ *rev7*Δ single or double mutations were constructed using appropriate pairs of ODN primers as described (Sambrook and Russell, 2001; Janke et al., 2004). Briefly, *REV7* gene was deleted using the KanMX4 (pFA6a- KanMX4) cassette with forward primer OSB11 and reverse primer OSB12. The loss of deleted gene was confirmed by PCR amplification using OSB13 and OSB14 primers. Similarly, other strains were constructed as follows: *MRE11* was deleted using the hphNT1 cassette (pYM-hphNT1) along with OSB52 and OSB54 primers; the loss of deleted gene was verified using the OSB53 probe. *REV1* was deleted using the hphNT1 cassette along with OSB55 and OSB56 primers; the loss of deleted gene was confirmed using the OSB57 probe. *REV3* was deleted using KanMX4 cassette (derived from pFA6a-hphNT1, pFA6a-KanMX4 respectively) along with OSB58 and OSB59 primers; the loss of deleted gene was confirmed using the OSB60 probe. The hphNT1 (pYM-hphNT1) cassette was used in the generation of double mutants (listed in *Supplementary Table S6*). The *rev7-C1* and *rev7-42* mutant strains were constructed by incorporating the sequences encoding the truncated species at the endogenous locus by using *rev7-C1*-9MYC-hphNT1 and *rev7-42*-3MYC-KANMX4 cassettes through overlapping primer-based PCR. The *rev7-C1*-9MYC-hphNT1 cassette was generated using primer pairs OSB116, OSB117 and OSB118, OSB70. Likewise, *rev7-42*-3MYC-KANMX4 cassette was generated using primer pairs OSB122, OSB120 and OSB121, OSB70. The N- and C-terminal truncation variants were confirmed using the probes OSB13 and OSB14, respectively.

Similarly, *mre11Δ, rev1Δ, rev3Δ,* and *rev7Δ* single knockout mutants were generated in the strain YW714 using hphNT1 cassette (derived from pFA6a-hphNT1). The *REV7* truncation variants - *rev7-C1-9MYC* and rev7-42 aa-3MYC - were generated as described above. *REV3* was deleted using hphNT1 cassette in strain PJ694A using OSB58 and OSB59 primers, and deletion was confirmed using primer OSB60 as the probe. Likewise, *mre11Δ rad50Δ xrs2Δ* triple knockout mutant was generated in strain PJ694A as follows: *mre11Δ::KANMX4* was generated by PCR-amplification of KANMX4 cassette (pFA6a-KANMX4) using OSB52 and OSB53 as forward and reverse primers, respectively, and deletion was confirmed using OSB54 as the probe. The *rad50Δ::URA3* strain was constructed by PCR amplification of URA3 cassette (pAG60-URA3) using primers OSB133 and OSB75, and deletion was

confirmed using OSB76 as the probe. Similarly, *xrs2Δ::HphNT1* was generated by PCR amplification of hphNT1 cassette (pFA6a-hphNT1) using primers OSB134 and OSB78, and deletion was confirmed using OSB79 as the probe.

Construction of DNA plasmids for expression and recombination assays

The plasmids FT10/Chr.IV$_{G4}$_lg and FT10/Chr.IV$_{G4}$_le were a kind gift from Dr. Virginia Zakian. *S. cerevisiae REV7* gene was amplified from genomic DNA by PCR using the primer pair (forward OSB01 and reverse OSB02) and Phusion DNA polymerase (NEB, Ipswich, MA) as described (Sambrook and Russell, 2001). This reaction yielded an amplicon of expected size, which was digested with BamHI/HindIII and ligated into a similarly digested pET28a(+) vector (Novagen) by utilizing the T4 DNA ligase. The resulting expression plasmid was designated pET-28a_REV7. In parallel, pET28a_ScREV7-C1 truncation was generated by PCR amplification of 609 bp (corresponding to the ScRev7-C1 truncation) using primers OSB01 and OSB125 using pET28a_ScREV7 plasmid DNA as template. The PCR product was digested with BamHI/HindIII and ligated into BamHI/HindIII digested pET28a vector. Likewise, *S. cerevisiae RAD50* gene was PCR-amplified from a genomic DNA preparation using OSB33 forward and OSB34 reverse primers. The amplicon was digested with BamHI/Xho1 and ligated into a similarly digested pE-SUMO Kan vector (Life Sensors, Malvern, PA) by utilizing the T4 DNA ligase. The resulting expression plasmid was designated pE-SUMO_*RAD50*. The *REV7*-eGFP expression vector was constructed by PCR amplification of the DNA fragment encoding the *S. cerevisiae REV7* gene in the pET-28a_*REV7* plasmid using forward Rev7-eGFP primer and reverse Rev7-eGFP primer (*Supplementary Table S6*). The amplicon of expected size was digested with XbaI/XhoI and ligated into a similarly digested pPROEX vector, upstream of eGFP coding sequence. The resulting plasmid encodes ScRev7-eGFP fusion protein. The pPROEX::eGFP vector was a kind gift from Deepak Saini.

The *ura3-G4* insert region was amplified by overlap extension PCR method using ODNs OSB80 and OSB82 as forward and OSB81 and OSB83 as reverse primers, respectively. The amplicon of expected size was digested with BamHI/SphI and ligated into a BamHI/Sph1 digested FAT10 vector. The ODN OSB82 corresponds to the DNA sequence 362751-362775 corresponding to the coding strand of *S. cerevisiae* Chr X and OSB81 is its complementary strand. Similarly, ura3-G4 mutant

was generated using ODNs OSB80 and OSB130 as forward, and OSB129 and OSB83 as reverse primers. The full-length ura3-G4 mutant PCR product was digested with BamHI/Sph1 and cloned into FAT10 vector. The ODNs OSB129 DNA sequence 362751-362775 corresponds to mutant version of *S. cerevisiae* Chr X and OSB130 is its complementary strand.

Construction of DNA plasmids for yeast two-hybrid analysis

To construct the pGBKT7-*REV7* the *S. cerevisiae REV7* orf in the pET28a (+) *REV7* construct was PCR-amplified by using Phusion DNA polymerase and forward OSB03 and reverse OSB04 primers, respectively. The amplicon of expected size was digested with Nde1/BamHI and ligated into a similarly digested pGBKT7 vector. The *S. cerevisiae MRE11* gene from genomic DNA was PCR-amplified using forward OSB05 primer and reverse *MRE11*_RP primer. The amplicon of expected size was digested with BamHI/EcoRI and ligated into the pGADT7 prey expression vector at the BamHI/EcoRI site. The same procedure was leveraged for the construction of all other prey expression vectors: *XRS2* was amplified from the genomic DNA using forward OSB36 and reverse OSB37 primers. The expected-size amplicon was digested with Nde1/BamHI and ligated into the pGADT7 prey expression vector at the Nde1/BamHI site; *RAD50* was amplified from the pESUMO_*RAD50* construct using forward OSB35 and reverse OSB34 primers. The expected-size amplicon was digested with EcoRI/Xho1 and ligated into the pGADT7 prey expression vector EcoRI/Xho1 site; *REV7* was amplified from the pET-28a_*REV7* construct using the same primers and ligated into pGADT7 prey expression vector as in the case of bait plasmid construction.

The N-terminally truncated ScREV7 variants (REV7- N1, REV7- N2, and REV7-N3) were constructed by PCR amplification of relevant portions of the *REV7* gene using OSB61, OSB62, OSB63 as a forward primer and OSB4 as a reverse primer (common for all N- terminal deletions), respectively. The C- terminally truncated ScREV7 variants (REV7-C1, REV7- C2 and REV7-C3) were constructed via PCR amplification of relevant portions of the *REV7* gene in the pET-28a_*REV7* plasmid using ODN OSB3 as a forward primer (common for all C-terminal deletions) and ODNs OSB64, OSB65 and OSB66 as reverse primers, respectively. The amplicons of expected size,

corresponding to the N- and C-terminal variants were digested with Nde1/BamHI and ligated into a similarly digested pGBKT7 vector. *S. cerevisiae* PJ694A strain was used in Y2H analyses.

Cell viability assay

S. cerevisiae wild type (WT) and isogenic mutant strains were grown in YPD or SC medium to an OD_{600} of 0.5. At this stage, ten-fold serial dilutions were spotted onto YPD agar plates with or without various concentrations of HU. Similarly, cells were spotted onto SC selective medium plates lacking appropriate amino acids, but with or without inhibitors, as indicated in figures/figure legends. The plates were incubated at 30 ºC for 3-4 days. The images were captured using epi-illumination at auto-exposure ChemiDoc MP imaging system (Bio-Rad).

Yeast two-hybrid interaction analysis

The Y2H assays were performed as previously described (Fields and Song, 1989; Thakur et al., 2020) Briefly, pairwise combination of plasmids expressing bait proteins, fused to the Gal4 DNA-binding domain (G4BD), and prey proteins, fused to the Gal4 activation domain (G4AD), were co-transformed into reporter WT strain PJ69-4A or its isogenic *rev3Δ* single or the *mre11Δ rad50Δ xrs2Δ* triple mutant strain. The empty prey vector and Rev7 expressing vector served as negative and positive controls respectively. The Y2H interactions were documented by spotting representative transformants onto SC/-Trp –Leu and SC/-Trp –Leu -His agar plates containing 15 mM 3-aminotrizole (3-AT), which were incubated for 3-5 days at 30°C. Growth of cells on SC-Leu-Trp-His +3-AT agar plates is indicative of moderate/strong protein-protein interactions between the bait and prey proteins.

Assay for G-quadruplex DNA/HU-induced toxicity

The assay was performed as previously described (Paeschke et al., 2011). The plasmid constructs used in this study were identical to the parent plasmid, pFAT10, except that its derivatives contain three tandem arrays of G sequences derived from

chromosome IV, inserted in the lagging or leading templates. Briefly, *S. cerevisiae* wild type, *rev7Δ* mutant, and cells expressing ScRev7 truncation variants (ScRev7-C1, ScRev7-42 aa) harboring the pFAT10 plasmid were synchronized in the G1 phase using α-factor at 30 °C and then released from the pheromone block by washing the cells. Subsequently, the cultures were normalized to equivalent A_{600} values, and tenfold serial dilutions of each culture was spotted onto solid SC/-Leu and SC/-Leu/+100 mM HU agar plates. The plates were incubated at 30 °C for 72 h.

Expression and purification of ScRev7

The *S. cerevisiae* MRX subunits were expressed and purified as previously described (Ghosal and Muniyappa, 2007). The *S. cerevisiae REV7* gene was sub-cloned into pET28a(+) expression vector with an N-terminal His_6-tag. The resulting plasmid was designated pET28a(+)_REV7. *E. coli* BL21(DE3)pLysS cells harboring pET28a(+)_REV7 plasmid were cultured in Luria-Bertani broth (1% tryptone, 0.5% yeast extract, 1% NaCl, pH 7.0) containing 50 μg/ml kanamycin at 37 °C with shaking at 180 rpm to an OD_{600} of 0.6. At that point, ScRev7 expression was induced by adding 1-thio-β-D-galactopyranoside (IPTG) to a final concentration of 0.1 mM. The IPTG-induced cultures were further incubated for 12 h at 25 °C. Cells were harvested by centrifugation at 6000 g the cell paste was resuspended in 50 ml of buffer A (20 mM Tris-HCl (pH 8.0), 150 mM NaCl, 10 % glycerol and 5 mM 2-mercaptoethanol containing 1 mM phenylmethylsulfonyl fluoride and 0.05 % Triton X-100). Cells were lysed by sonication on ice (7 x 1-min pulses) and quickly subjected to centrifugation at 30,000 rpm, 4°C for 20 min. Solid ammonium sulfate was added (0.472 gm/ml) to the supernatant with continuous stirring for 45 min at 24 °C. The precipitate was collected by centrifugation at 18000 rpm at 4°C for 1 h. The precipitate was dissolved in buffer A and dialyzed against the same buffer. The dialysate was loaded onto 5 ml Ni^{2+}-NTA column (Qiagen, Valencia, CA). After washing the column with buffer A containing 20 mM imidazole, bound proteins were eluted with a gradient of 20→500 mM imidazole. The fractions containing ScRev7 were pooled and dialyzed against buffer B (20 mM Tris-HCl, pH 8.0, 1.2 M NaCl, 7 % glycerol, 5 mM 2-mercaptoethanol). It was further purified by chromatography on a Superdex S75 column attached to an AKTA Prime FPLC system, which had been equilibrated with and eluted using buffer B. The

peak fractions containing ScRev7 were pooled and dialyzed against buffer C (20 mM Tris-HCl (pH 8.0), 30 mM NaCl, 30 % glycerol, 5 mM 2-mercaptoethanol), and loaded onto a heparin column (5 ml). The bound proteins were eluted with a gradient of 30→350 mM NaCl in buffer C. An aliquot from each eluted fraction was visualized by staining with Coomassie Brilliant Blue R250 after SDS-PAGE. The fractions that contained ScRev7 were pooled and dialyzed against buffer D (20 mM Tris-HCl (pH 8.0), 100 mM NaCl, 10 % glycerol, 1 mM DTT), and stored at -80 °C.

Expression and purification of ScRev7-eGFP

The His_6-tagged ScRev7-eGFP fusion protein was expressed in and purified from whole cell lysates of *E. coli* BL21(DE3)pLysS host strain harboring the pPROEX/REV7-eGFP plasmid as described above. The His_6-tagged eGFP was purified from the cell lysates of *E. coli* BL21* (DE3) pLysS host strain harboring eGFP pPROEX expression plasmid by Ni^{2+}-NTA affinity chromatography. Briefly, the whole cell lysate was loaded onto the Ni^{2+}-NTA resin column (5 ml), which had been equilibrated with a buffer A (HEPES, pH 7.5, 50 mM NaCl and 10% glycerol). The column was washed with buffer A containing 70 mM imidazole. The bound proteins were eluted with a gradient of 70 → 800 mM imidazole in buffer A. An aliquot from each eluted fraction was analyzed by SDS-PAGE and visualized by staining with Coomassie Brilliant Blue R250. The protein concentrations were determined by the Bradford assay. The fractions that contained ScRev7-eGFP and eGFP were pooled, dialyzed against buffer A, and stored at -80 °C.

Expression and purification of *S. cerevisiae* Rev1

The GST-tagged Rev1 was purified as described previously with certain modifications (Johnson et al., 2006). Briefly, *S. cerevisiae* BJ5464 cells bearing plasmid pBJ842-Rev1-GST were selected on SC plates lacking leucine. Single colonies were inoculated into SC/-Leu liquid media (200 ml) containing 2% raffinose for 12-14 h at 30°C until they reached an optical density (OD) at 600 nm reached 0.1. The cultures were incubated at 250 rpm, 30°C, till the $O.D_{600nm}$ is equal to 0.5. Following this, the cultures were centrifuged at 4000 rpm for 10 min and the pellet was washed thrice

with MilliQ water. Cells were then resuspended into SC/-Leu media containing 2% galactose. The cultures were further incubated at 30 °C/250 rpm for 7 h. The cells were harvested by centrifugation at 4000 rpm for 10 min, resuspended in CBB buffer (50 mM Tris-HCl pH 7.5, 10% sucrose, 1 mM EDTA, 10 mM β-mercaptoethanol and 5 μg/mL of protease inhibitor cocktail). Cells were lysed using a FastPrep 24 homogenizer. Following lysis, the cell debris was separated by centrifugation at 10,000 rpm for 10 min. The supernatant was further cleared by centrifugation at 35000 rpm for 30 min. The GST-tagged protein was precipitated from the cell lysate using ammonium sulfate (0.208 g/ml), followed by centrifugation at 20,000 rpm for 45 min. The pellet was resuspended in the GST-binding buffer (GBB, 50 mM Tris-HCl pH 7.5, 10% glycerol, 1 mM EDTA, 10 mM β-mercaptoethanol and 5 μg/mL of protease inhibitor cocktail) and dialyzed extensively against the same buffer. The sample was then loaded onto the GST-column (GSTrap High performance column, 5 ml, Cytiva Life Sciences), loaded at the rate of 0.5 mL/min. The column was then washed with GBB buffer containing 500 mM NaCl, to remove non-specific interactors. Bound protein was eluted into 30 fractions (1 mL each) at a flow rate of 1 mL/min in GBB buffer containing 40 mM glutathione. The fractions were analysed on 10% SDS-PAGE, followed by Coomassie staining, and the fractions containing purified Rev1-GST protein were pooled and dialysed against MST buffer (HEPES, pH 7.5, 50 mM NaCl, 10% glycerol), and stored at -80°C. The concentration of ScRev7 and its derivatives was determined by the dye-binding assay.

SDS-PAGE and Immunoblot analysis

Conventional protocols were employed for SDS-PAGE and immunoblotting using a polyvinylidene difluoride (PVDF) membrane was performed as described (Mahmood and Yang, 2012). The *S. cerevisiae* PJ69-4A strains were co-transformed with empty vectors pGBKT7 and pGADT7, or a bait vector harboring Rev7 truncations in combination with prey vectors harboring *REV7*, *MRE11*, *XRS2* or *RAD50*. The transformants were selected by plating onto SC/-Leu,-Trp medium, and single colonies were inoculated into 5 ml SC/ -Trp,-Leu media containing 2% dextrose. The cells were grown at 30°C for 12-14h at 250 rpm to OD_{600nm} = 0.15, which were then transferred onto 10 ml of SC/ -Trp,-Leu medium. Incubation was continued at 250

rpm/30°C to OD_{600nm} = 0.5 to 0.6. The cells were harvested by centrifugation at 4000 rpm for 5 min and the pellet was resuspended using lysis buffer (50 mM sodium-HEPES pH 7.5, 200 mM sodium acetate pH 7.5, 1 mM EDTA, 1 mM EGTA, 5 mM magnesium acetate and 5% glycerol). Cells were lysed with 2 min. bursts at 4.0 m/s on a FastPrep-24 homogenizer in the presence of 200 ml of acid-washed glass beads. The samples were centrifuged at 7000 rpm for 5 min to remove the beads and cell debris. The supernatant was further centrifuged at 13000 rpm for 10 min. Fifty micrograms of proteins were separated by10% SDS-PAGE. Then, proteins were transferred to 0.45 µm PVDF membranes, followed by blocking for 1 h at 25°C with 5% nonfat dry milk in TBST (20 mM Tris–HCl buffer, pH 7.5,150 mM NaCl, 0.1% Tween 20) buffer. The blot was rinsed with TBST twice and incubated with anti-myc antibodies (diution 1:3000 dilution) for 1 h at 25 °C. The blots were washed thrice with TBST buffer and incubated with HRP-conjugated anti-rabbit antibodies (dilution 1:20000; Sigma-Aldrich) at 25°C for 1 h. Following incubation, the blots were washed thrice with TBST buffer and developed using chemiluminescence substrates (Bio-Rad Laboratories, CA, USA) in the Bio-Rad ChemiDoc Imaging systems. Anti-PGK1 antibodies were obtained from Santa-Cruz Biotechnologies, CA, USA.

Structure prediction of heterodimer protein complexes

The sequences of full-length ScRev7, Mre11 and Rad50 were obtained from the *Saccharomyces* Genome Database (https://www.yeastgenome.org/). Structural models for the complexes between ScRev7-Mre11 and ScRev7-Rad50 were built using publicly available versions of AlphaFold-Multimer algorithm (Evans et al., 2022; Varadi et al., 2022) and ColabFold software (Mirdita et al., 2022) to run AlphaFold-Multimer (https://github.com/sokrypton/ColabFold). The models with the highest confidence were analysed using LigPLot software, Version 2.2, to detect the amino acid residues involved in the interactions between the Mre11/Rad50 subunits and ScRev7. Approximately, 44% and 43% of the residues across the binding interface of ScRev7 and Mre11 displayed confident pLDDT scores greater than 60. Similarly, 67% and 100% of the residues lining the ScRev7 and Rad50 interface exhibited pLDDT scores greater than 60. The PyMOL Molecular Graphics System, Version 2.5.5, was used for visualizing the structures. Of the 5 models generated by

AlphaFold-Multimer, the top models (based on average pLDDT score) were chosen for display.

Microscale thermophoresis assay

MicroScale Thermophoresis (MST) assay was performed on a Monolith NT.115 instrument (NanoTemper Technologies GmbH) according to the manufacturer's instructions. Samples were prepared in 20 µl MST buffer (HEPES, pH 7.5, 50 mM NaCl, 10% glycerol) and ScRev7-eGFP or eGFP and with varying concentrations of ligands (Mre11, Rad50 or Xrs2) in the following concentration range: Mre11 (0.00015 to 5 µM), Rad50 (0.00006 to 2 µM), Xrs2 (0.00015 to 5 µM) or Rev1 (0.00015 to 5 µM). After incubation at 37 ºC for 15 min, samples were transferred into Monolith NT.115 glass capillaries and and MST measurements were performed using 40% MST power with laser on/off times of 30 s and 5 s. MST signals were normalised to fraction bound (X) by X= [Y(c)− Min]/(Max − Min), error bars (SD) were normalized by stdnorm = std(c)/(Max − Min). The Fnorm values were plotted against the ligand concentration, to obtain an estimate of binding affinity. The K_d values and Hill coefficients (n_H) were calculated using MO Affinity Analysis software (NanoTemper). All data were statistically analyzed and graphed using GraphPad Prism software (v5.0).

Preparation of radiolabeled DNA substrates

The sequences of and oligonucleotides (ODNs) used for the preparation of substrates are listed in *supplementary Table S7*.The ODNs were labeled at the 5' end using [γ-^{32}P]ATP and T4 polynucleotide kinase as described (Sambrook and Russell, 2001). The unincorporated [γ-^{32}P]ATP was removed using a Sephadex G-50 superfine mini-column. The ^{32}P-labeled G-quadruplexes were prepared by incubating the G-rich containing single-stranded ODNs (OSB28, OSB92 and ODN6G3) in annealing buffer [10 mM Tris-HCl (pH 8.0), 1 mM EDTA and 120 mM KCl] by heating at 95 °C for 2 min and then slowly cooling down to 24 °C. These ODNs contain arrays of G residues, which adopt thermally stable G4 topologies (Muniyappa et al., 2000). The dsDNA substrates were prepared as follows: 41-bp dsDNA by mixing aliquots of 5'-end ^{32}P-labeld OSB17 (upper strand) with a small

excess of unlabeled complementary OSB20; 60-bp dsDNA by mixing OSB41 (upper strand) and OSB42 (lower strand) in 1X SSC buffer (0.3 M sodium citrate buffer, pH 7.0, containing 3 M NaCl), followed by heating at 95 °C for 5 min and then slowly cooling to 24 °C over a period of 90 min. The substrates were resolved by non-denaturing 8% PAGE for 4 h at 4 °C. Finally, the dsDNA substrates were eluted from the gel slices in TE buffer (10 mM Tris-HCl, pH 7.5, and 1 mM EDTA) and stored at 4 °C for further use.

Electrophoretic mobility shift assay

The electrophoretic mobility shift assays (EMSA) were performed as previously described (Thakur et al., 2021). The reaction mixtures (20 μl), which contained 20 mM Tris-HCl (pH 7.5), 0.1 mM DTT, 0.2 μg/ml BSA and 5% glycerol), 0.5 nM of the specified ^{32}P-labeled DNA substrate and increasing concentrationsof ScRev7/ScRev7-C1 as indicated in the figure legends. After incubation at 37 °C for 90 min, 2 μl gel-loading solution (0.1% of bromophenol blue and xylene cyanol in 20% glycerol) was added to each sample. The samples were loaded onto a non-denaturing 4% polyacrylamide gel. Electrophoresis was performed in 45 mM Tris-borate buffer (pH 8.3) containing 10 mM KCl and 1 mM EDTA, initially at 150 V for 20 min, and then at 10 V/cm at 4°C for 3 h. The bands were visualized using a Fuji FLA-9000 phosphor imager analyzer and quantified using UVI-Band Map software (v. 97.04). The binding curves were submitted to a nonlinear regression curve analysis using the software GraphPad Prism software (version 5.0). The values were calculated by using the equation $Y = B_{max} X/(Kd + X)$.

AsCas12a exonuclease assay

The assay was performed as previously described (Arora et al., 2017) with slight modifications. Two steps are involved in the assay: first, assembly of the ScRev7-MRX complex and second, nuclease susceptibility assay. The MRX subunits (100 nM each) were mixed with increasing concentrations of ScRev7 (0.05 to 2.5 μM) or ScRev7-C1 (1.5 and 3 μM) and incubated on ice for 15 min, prior to the addition of

20 μl of reaction mixture that contained 25 mM MOPS (pH 7.0), 20 mM Tris-HCl (pH 7.5), 80 mM NaCl, 8% glycerol, 5 mM $MnCl_2$, 0.1 mM DTT, 200 μg/ml BSA and 10 nM of ^{32}P-labeled 60-bp dsDNA. Subsequently, the reaction mixtures were incubated at 37 °C for 1 h, and the reaction stopped by adding a 2 μl solution containing 2 mg/ml proteinase K, 50 mM EDTA and 1% SDS. After incubation at 37 °C for 30 min, 5 μl of a solution containing 10 μg/ml glycogen, 2 μl 3 M sodium acetate and 50 μl of absolute ethanol was added to each sample and were frozen at -80°C. The thawed samples were centrifuged at 15000 rpm at 4 °C for 30 min. The pellets were washed with 70% ethanol and centrifuged at 15000 rpm at 4 °C for 5 min. The dried pellets were resuspended in 10 μl gel-loading dye (80% formamide, 10 mM EDTA, 0.1% xylene cyanol and 0.1% bromophenol blue) and then incubated at 95 °C for 5 min. Aliquots were loaded onto an 8% denaturing polyacrylamide/7 M urea gel. Electrophoresis was performed in TBE buffer (89 mM Tris-borate (pH 8.3) and 1 mM EDTA) for 2 h at 40 W. The dried gel was visualized using a Fuji FLA 9000 phosphor imager.

AsCas12a endonuclease assay

The assay was carried out as previously described (Shibata et al., 2014) with slight modifications. Briefly, the reaction mixtures (10 µl) without ScRev7 contained 100 ng of M13 circular ssDNA, 30 mM Tris-HCl, pH 7.5, 25 mM KCl, 5 % glycerol, 1 mM DTT, 200 µg/ml BSA, 5 mM $MnCl_2$ and increasing concentrations of ScMre11 (0.1-2 µM). After incubation at 37 °C for 1 h, the reaction was quenched by adding 2 μl of stop solution (2 mg/ml proteinase K, 50 mM EDTA and 1 % SDS) and incubation was extended for 30 min. The reactions were quenched by adding 2 µl of gel-loading solution. The reaction products were separated by electrophoresis on a 0.8% native agarose gel using 44.5 mM Tris-borate buffer (pH 8.3) containing 0.5 mM EDTA at 10 V/ cm for 1 h. The gel was stained with ethidium bromide and the image was captured using the UVItec gel documentation system (UVItec, Cambridge, UK). To test the effect of ScRev7 on Mre11 endonuclease activity, the assay was carried out as described above, except that the ScRev7-Mre11 heterodimer was first formed by incubating with increasing concentration of ScRev7 on ice for 15 min, prior to the addition of 10 μl of reaction mixture. The reaction mixtures were incubated and

processed as described above.

ATP crosslinking assay

The assay was carried out as previously described (Thakur et al., 2021). To test for the effect of ScRev7 on ATP binding by Rad50, we first ascertained its capacity to bind ATP. The assay was performed in a 20 µl reaction mixture containing 50 mM Tris-HCl (pH 5.0), 10 mM $MgCl_2$, 400 pmol [γ-^{32}P]ATP and increasing concentrations of Rad50 (0.1-1 µM). In parallel, a fixed concentration of Rad50 (1 µM) was incubated with increasing concentrations of ScRev7 (0.5 - 6 µM) at 4 °C for 15 min, prior to mixing with 20 µl buffer containing 50 mM Tris-HCl (pH 5.0), 10 mM $MgCl_2$ and 400 pmol [γ-^{32}P]ATP. After incubation at 4 °C for 25 min, samples were exposed to UV irradiation (1.2×10^5 µJ/cm^2 in Hoefer UVC 500 ultraviolet crosslinker) at a distance of 2 cm. All cross-linking reactions were quenched by adding 5 µl of 5X Laemmli buffer (10 mM Tris-HCl, pH 6.8, 12.5% SDS, 40% glycerol, and 0.1% bromophenol blue). Samples were heated at 95 °C for 10 min and resolved by SDS/PAGE in 10% polyacrylamide gel at 35 mA for 2 h. The images were captured using a Fuji FLA-9000 phosphor imager and the band intensities of radiolabeled species was quantified using UVI-Band Map software (v. 97.04) and graphs were plotted using GraphPad Prism software (v5.0).

ATPase assay

The hydrolysis of ATP by ScRad50 was monitored by the release of ^{32}Pi from [γ-^{32}P]ATP as described (Thakur et al., 2021). Where indicated, a fixed concentration of Rad50 (0.5 µM) was incubated on ice for 30 min with increasing concentrations of ScRev7 or ScRev7-C1 to allow protein complex formation, prior to the reaction. Briefly, 200 µM [γ–^{32}P] ATP and Rad50 (0.5 µM) were incubated in 10 µl reaction mixture containing 20 mM Tris HCl (pH 7.5), 50 mM KCl, 0.2 mg/ ml BSA, 0.1 mM DTT, 1.0 mM $MgCl_2$ and 5 % glycerol, with indicated concentrations of Rad50. The reactions were carried out at 30 °C for 30 min and the reaction was quenched by adding 15 mM EDTA. Aliquots (2 µl) from each sample was spotted onto the PEI-cellulose thin-layer plate and was developed using a solution containing 0.5 M LiCl, 1

M formic acid and 1 mM EDTA as the mobile solvent. The TLC sheets were dried and the autoradiographs were visualized using Fuji FLA-9000 phosphor imager. The images were captured using a Fuji FLA-9000 phosphor imager and the band intensities of ^{32}Pi and [γ-^{32}P]ATP were quantified and plotted using UVI-Band map software. The isotherms were generated by non-linear regression analysis using GraphPad Prism (Version 5.0).

Malachite green phosphate assay

ATP hydrolysis was monitored by measuring the amount of inorganic phosphate released using acidic ammonium molybdate and malachite green assay (Lanzetta et al., 1979). The reaction mixtures (80 µl) contained 20 mM Tris-HCl, pH 7.5, 50 mM KCl, 5% glycerol, 0.1 mM DTT, 0.2 mg/ml BSA, 1 mM $MgCl_2$, 150 µM ATP, and increasing concentrations of ScRad50 (0.05 - 1 µM). After incubation at 30°C for 30 min, reaction was stopped by adding 20 µl of malachite green reagent (Sigma-Aldrich, MAK307). Incubation was continued for 15 min at 24°C to allow the formation of phosphomolybdate malachite green chromogenic complex. The absorbance values, as a measure of the extent of ATP hydrolysis, at 620 nm (y-axis) were plotted against increasing concentrations of ScRad50 (x-axis). To test the effect of ScRev7 or ScRev7-C1 on Rad50 ATPase activity, increasing concentrations of ScRev7 or ScRev7-C1 (0, 0.1, 0.3, 0.5, 1, 1.5, 2 µM) were incubated with 0.25 µM of ScRad50 on ice for 20 min, prior to mixing it with the reaction mixture. After incubation at 30 °C for 30 min, ATP hydrolysis was monitored as described above. The curves were fitted using non-linear regression analysis using GraphPad prism (v. 5.0).

Mass spectrometry analysis

Identity of Rev7-GFP protein was confirmed using Orbitrap mass spectrometry method (Zubarev and Makarov, 2013). In-gel trypsin digestion was performed as follows: 50 mM ammonium bicarbonate and acetonitrile (7:3) ratio was used for de-staining; following which, samples were reduced for 30 minutes by adding 10 mM DTT diluted in 50 mM ammonium bicarbonate. Following reduction, alkylation buffer (55 mM iodoacetamide in 50 mM ammonium bicarbonate) was added and samples were incubated at room temperature for further 30 min. Samples were treated with 10 ng

trypsin enzyme (Mass spectrometry-grade, Sigma Aldrich, India), at 37°C for 12 h. Subsequently, peptides were extracted from the sample by desalting with 300 µL of 70% acetonitrile containing 0.1% trifluoracetic acid. The extracted peptides are dried in speed vacuum and resuspended in 40 µL resuspension buffer (2% acetonitrile in LC-MS grade Milli-Q). 10 µL of the sample was then injected into Orbitrap Fusion Tribid Mass spectrometer (Thermo Fisher Scientific Inc., USA). Samples were run for 110 minutes using Nanospray Ion source (NSI) and static spray voltage. Ions were detected by Orbitrap detector at 60000 resolution using quadrupole isolation. Daughter ions were detected by Ion Trap detector using quadrupole isolation mode. Following data acquisition, peptide spectrum matches (PSMs) and percentage peptide coverage were obtained for the samples. Collectively, these results confirm that the purified protein is GFP-tagged ScRev7.

Non-homologous end-joining assayed using linear plasmid substrate

The role of *S. cerevisiae REV*7 alone and in combination with various genes in NHEJ was assessed using a linear plasmid re-circularization assay as described (Zhang and Paull, 2005; Ghodke and Muniyappa, 2013). Briefly, 60 ng of BamHI-digested or undigested plasmid pRS416 was transformed into the WT and isogenic *rev1*Δ*, rev3*Δ*, rev7*Δ, *mre11*Δ*, sae2*Δ*, rev1*Δ*rev3*Δ*, rev1*Δ*rev7*Δ*, rev3*Δ*rev7*Δ*, mre11*Δ*rev7*Δ*, sae2*Δ*rev7*Δ *rev7-C1* or *rev7-42* strains. In these experiments, the uncut plasmid pRS416 served as a control. The transformants arising from plasmid re-circularization were selected on SC/-Ura plates after growth at 30 °C for 3-5 days. The efficiency of transformation was calculated as a ratio of the number of transformants with digested plasmid DNA to that with undigested plasmid DNA. The graph was obtained using GraphPad Prism (Version 5.0) and statistical significance was calculated using one-way ANOVA Dunnett's multiple comparisons test.

Non-homologous end-joining using "suicide deletion" reporter assay

The assay was performed as described (Karathanasis and Wilson, 2002). Briefly, single colonies of *S. cerevisiae* YW714 strains *WT*, *rev1*Δ*, rev3*Δ*, rev7*Δ, *mre11*Δ*, ku70*Δ*, rev7-C1 and rev7-42* were inoculated into SC/-Ura liquid media for 30h, at 30°C, 250 rpm. The cells were harvested by centrifugation at 4000 rpm for 10 min.

Cell pellets were washed thrice with MilliQ water and resuspended in SC media at O.D.$_{600}$ equal to 1. Following this, appropriate serial dilutions were plated parallelly onto SC/-Ura plates containing glucose and SC/-Ade plates containing galactose. The plates were incubated at 30°C for 5 days and the numbers of colonies were counted on both sets of plates for each strain. The rate of NHEJ, as a function of Ade$^+$ colonies was calculated using the FALCOR software (Hall et al., 2009) for three independent experiments. The differences between experimental results and relevant controls were tested with Dunnett's multiple comparison test. The graph was generated using GraphPad Prism (Version 5.0). Statistical tests and p-values are mentioned in each figure legend.

Plasmid-chromosome recombination assay

The assay was performed as previously described (Paeschke et al., 2013). The WT and isogenic *ura3-1, ura3-1 rev7Δ, ura3-1 mre11-D56N,H125N ura3-1 rev7Δ mre11-D56N,H125N, ura3-1 rev7-C1* and *ura3-1 rev7-42* strains were transformed with 60 ng of empty vector (pFAT10) or a plasmid bearing G4 DNA capable sequences (pFAT10-G4) (Paeschke et al., 2011). The synchronous cells were grown in SC/-Leu medium to OD_{600} = 0.5. At this stage, equal number of cells were replica-spotted onto the SC/-Ura medium (left) and SC/-Ura medium supplemented with 0.1 M HU (right). Plates were incubated at 30 °C for 4-6 days. The recombination frequency was calculated as described (Hall et al., 2009).

Statistical and data analysis

Statistical comparison of two groups was evaluated using the one-way ANOVA Dunnett's multiple comparison test or Tukey's post hoc analysis. Statistical significance level was set as follows: *, P-value < 0.05; **, P-value < 0.01; ***, P-value < 0.001; ****, P-value < 0.0001. Unless otherwise specified, details of statistical methods used to analyse the data are provided in the Legends to the Figures. No data was excluded from analysis.

Acknowledgements

We thank Drs. Virginia Zakian, Maria Pia Longhese, Lorraine Symington and Thomas Wilson for kindly providing some of the strains used in this study, as well as to Dr. Narottam Acharya for the generous gift of ScRev7 and ScRev1 expression plasmids, *S. cerevisiae* BJ5464 strain and for his assistance in the purification of expressed proteins, and to Naren Chandran Shakthivel for his assistance with the generation of AlphaFold-Multimer models.

Funding

This work was supported by a grant (CRG/2021/000082) from the Science and Engineering Research Board, New Delhi to K. M., who was also the recipient of Bhatnagar Fellowship (SP/CSIR/425/2018) from the council of Scientific and Industrial Research, New Delhi.

Author contributions

Sugith Badugu, Kshitiza M. Dhyani, Manoj Thakur: Investigation, Methodology, Software, Validation, Data curation, Writing – original draft and editing; Kalappa Muniyappa, Conceptualization, Resources, Supervision, Funding acquisition, Formal analysis, Project administration, Writing – review and editing.

Conflict of interest statement

None declared

Data availability

All data associated with this study are in the article.

REFERENCES

Acharya N, Johnson RE, Prakash S, Prakash L. 2006. Complex formation with Rev1 enhances the proficiency of *Saccharomyces cerevisiae* DNA polymerase zeta for mismatch extension and for extension opposite from DNA lesions. *Molecular and Cellular Biology* **26**: 9555-9563.

Arora S, Deshpande RA, Budd M, Campbell J, Revere A, Zhang X, Schmidt KH, Paull TT. 2017. Genetic separation of Sae2 nuclease activity from Mre11 nuclease functions in budding yeast. *Molecular and Cellular Biology* **37**: e00156-17.

Baranovskiy AG, Lada AG, Siebler HM, Zhang Y, Pavlov YI, Tahirov TH. 2012. DNA polymerase delta and zeta switch by sharing accessory subunits of DNA polymerase delta. *The Journal of Biological Chemistry* **287**: 17281–17287.

Bezalel-Buch R, Cheun YK, Roy U, Schärer OD, Burgers PM. 2020. Bypass of DNA interstrand crosslinks by a Rev1-DNA polymerase ζ complex. *Nucleic Acids Research* **48**: 8461-8473.

Bluteau D, Masliah-Planchon J, Clairmont C, Rousseau A, Ceccaldi R, Dubois d'Enghien C, Bluteau O, Cuccuini W, Gachet S, Peffault de Latour R, *et al*. 2016. Biallelic inactivation of REV7 is associated with Fanconi anemia. *The Journal of Clinical Investigation* **126**: 3580–3584.

Boersma V, Moatti N, Segura-Bayona S, Peuscher MH, van der Torre J, Wevers BA, Orthwein A, Durocher D, Jacobs JJL. 2015. MAD2L2 controls DNA repair at telomeres and DNA breaks by inhibiting 5' end resection. *Nature* **521**: 537–540.

Boulton SJ, Jackson SP. 1998. Components of the Ku-dependent non-homologous end-joining pathway are involved in telomeric length maintenance and telomeric silencing. *The EMBO Journal* **17**: 1819–1828,

Capra JA, Paeschke K, Singh M, Zakian VA. 2010. G-quadruplex DNA sequences are evolutionarily conserved and associated with distinct genomic features in *Saccharomyces cerevisiae*. *PLoS Computational Biology* **6**: e1000861.

Casari E, Rinaldi C, Marsella A, Gnugnoli M, Colombo CV, Bonetti D, Longhese MP. 2019. Processing of DNA double-strand breaks by the MRX complex in a chromatin context. *Frontiers in Molecular Biosciences* **6**: 43.

Castillo Bosch P, Segura-Bayona S, Koole W, van Heteren JT, Dewar JM, Tijsterman M, Knipscheer P. 2014. FANCJ promotes DNA synthesis through G-quadruplex structures. *The EMBO Journal* **33**, 2521–2533.

Cejka P, Symington LS. 2021. DNA End resection: mechanism and control. *The Annual Review of Genetics* **55**: 285-307.

Clairmont CS, D'Andrea AD. 2021. REV7 directs DNA repair pathway choice. *Trends in Cell Biology* **31**: 965-978.

Clairmont CS, Sarangi P, Ponnienselvan K, Galli LD, Csete I, Moreau L, Adelmant G, Chowdhury D, Marto JA, D'Andrea AD. 2020. TRIP13 regulates DNA repair pathway choice through REV7 conformational change. *Nature Cell Biology* **22**: 87–96.

Dai Y, Zhang F, Wang L, Shan S, Gong Z, Zhou Z. 2020. Structural basis for shieldin complex subunit 3-mediated recruitment of the checkpoint protein REV7 during DNA double-strand break repair. *The Journal of Biological Chemistry* **295**: 250–262.

De Krijger I, Boersma V, Jacobs JJL. 2021. REV7: Jack of many trades. *Trends in Cell Biology* **31**: 686-701.

Decottignies A. 2013. Alternative end-joining mechanisms: a historical perspective. *Frontiers in genetics* **4**: 48.

Dev H, Chiang TW, Lescale C, de Krijger I, Martin AG, Pilger D, Coates J, Sczaniecka-Clift M, Wei W, Ostermaier M, *et al*. 2018. Shieldin complex promotes DNA end-joining and counters homologous recombination in BRCA1-null cells. *Nature Cell Biology* **20**: 954–965.

Du Truong C, Craig TA, Cui G, Botuyan MV, Serkasevich RA, Chan KY, Mer G, Chiu PL, Kumar R. 2021. Cryo-EM reveals conformational flexibility in apo DNA polymerase ζ. *The Journal of Biological Chemistry* **297**, 100912.

Estep KN, Butler TJ, Ding J, Brosh RM. 2019. G4-interacting DNA helicases and polymerases: potential therapeutic targets. *Current Medicinal Chemistry* **26**: 2881–2897.

Evans R, O'Neill M, Pritzel A, Antropova N, Senior A, Green T, *et al*. 2022. Protein complex prediction with AlphaFold-Multimer. *bioRxiv.* https://doi.org/10.1101/2021.10.04.463034 24.

Fields S, Song O. 1989. A novel genetic system to detect protein-protein interactions. *Nature* **340**: 245–246.

Findlay S, Heath J, Luo VM, Malina A, Morin T, Coulombe Y, Djerir B, Li Z, Samiei A, Simo-Cheyou E, *et al*. 2018. SHLD2/FAM35A co-operates with REV7 to coordinate DNA double-strand break repair pathway choice. *The EMBO Journal* **37**: e100158.

Gao S, Feng S, Ning S, Liu J, Zhao H, Xu Y, Shang J, Li K, Li Q, Guo R, *et al*. 2018. An OB-fold complex controls the repair pathways for DNA double-strand breaks. *Nature Communications* **9**: 3925.

Ghezraoui H, Oliveira C, Becker JR, Bilham K, Moralli D, Anzilotti C, Fischer R, Deobagkar-Lele M, Sanchiz-Calvo M, Fueyo-Marcos E, *et al*. 2018. 53BP1 cooperation with the REV7-shieldin complex underpins DNA structure-specific NHEJ. *Nature* **560**: 122–127.

Ghodke I, Muniyappa K. 2013. Processing of DNA double-stranded breaks and intermediates of recombination and repair by *Saccharomyces cerevisiae* Mre11 and its stimulation by Rad50, Xrs2, and Sae2 proteins. *The Journal of Biological Chemistry* **288**: 11273–11286.

Ghosal G, Muniyappa K. 2005. *Saccharomyces cerevisiae* Mre11 is a high-affinity G4 DNA-binding protein and a G-rich DNA-specific endonuclease: implications for replication of telomeric DNA. *Nucleic Acids Research* **33**: 4692–4703.

Ghosal G, Muniyappa K. 2007. The Characterization of *Saccharomyces cerevisiae* Mre11/Rad50/Xrs2 complex reveals that Rad50 negatively regulates Mre11 endonucleolytic but not the exonucleolytic activity. *The Journal of Molecular Biology* **372**: 864–882.

Gómez-Llorente Y, Malik R, Jain R, Choudhury JR, Johnson RE, Prakash L, Prakash S, Ubarretxena-Belandia I, Aggarwal AK. 2013. The architecture of yeast DNA polymerase ζ. *Cell Reports* **5**: 79–86.

Guo C, Fischhaber PL, Luk-Paszyc MJ, Masuda Y, Zhou J, Kamiya K, Kisker C, Friedberg EC. 2003. Mouse Rev1 protein interacts with multiple DNA polymerases involved in translesion DNA synthesis. *The EMBO Journal* **22**: 6621–6630.

Gupta R, Somyajit K, Narita T, Maskey E, Stanlie A, Kremer M, Typas D, Lammers M, Mailand N, Nussenzweig A, *et al*. 2018. DNA repair network analysis reveals shieldin as a key regulator of NHEJ and PARP inhibitor sensitivity. *Cell* **173**: 972–988.

Hall BM, Ma C-X, Liang P, Singh KK. 2009. Fluctuation analysis CalculatOR: a web tool for the determination of mutation rate using Luria-Delbruck fluctuation analysis. *Bioinformatics* **25**: 1564–1565.

Haracska L, Unk I, Johnson RE, Johansson E, Burgers PM, Prakash S, Prakash L. 2001. Roles of yeast DNA polymerases delta and zeta and of Rev1 in the bypass of abasic sites. *Genes & Development* **15**: 945–954.

Hoff B, Kamerewerd J, Sigl C, Mitterbauer R, Zadra I, Kürnsteiner H, Kück U. 2010. Two components of a velvet-like complex control hyphal morphogenesis, conidiophore development, and penicillin biosynthesis in *Penicillium chrysogenum. Eukaryotic Cell*. **9**:1236-50.

Huang ME, Rio AG, Galibert MD, Galibert F. 2002. Pol32, a subunit of *Saccharomyces cerevisiae* DNA polymerase delta, suppresses genomic deletions and is involved in the mutagenic bypass pathway. *Genetics* **160**: 1409–1422.

Huber MD, Lee DC, Maizels N. 2002. G4 DNA unwinding by BLM and Sgs1p: substrate specificity and substrate-specific inhibition. *Nucleic Acids Research* **30**: 3954-3961.

Huppert JL, Balasubramanian S. 2005. Prevalence of quadruplexes in the human genome. *Nucleic Acids Research* **33**: 2908-2916.

James P, Halladay J, Craig EA. 1996. Genomic libraries and a host strain designed for highly efficient two-hybrid selection in yeast. *Genetics* **144**: 1425–1436.

Janke C, Magiera MM, Rathfelder N, Taxis C, Reber S, Maekawa H, Moreno- Borchart A, Doenges G, Schwob E, Schiebel E, Knop M. 2004. A versatile toolbox for PCR-based tagging of yeast genes: new fluorescent proteins, more markers and promoter substitution

cassettes. *Yeast* **21**: 947–962.
Johnson RE, Prakash L, Prakash S. 2006. Yeast and human translesion DNA synthesis polymerases: expression, purification, and biochemical characterization. *Methods in Enzymology* **408**: 390-407.
Johnson RE, Prakash L, Prakash S. 2012. Pol31 and Pol32 subunits of yeast DNA polymerase delta are also essential subunits of DNA polymerase zeta. *Proceedings of the National Academy of Sciences USA* **109**: 12455–12460.
Karathanasis E, Wilson WT. 2002. Enhancement of *Saccharomyces cerevisiae* end-joining efficiency by cell growth stage but not by impairment of recombination. *Genetics* **161**: 1015–1027.
Kikuchi S, Hara K, Shimizu T, Sato M, Hashimoto H. 2012. Structural basis of recruitment of DNA polymerase ζ by interaction between REV1 and REV7 proteins. *The Journal of Biological Chemistry* **287**: 33847-33852.
Kochenova OV, Bezalel-Buch R, Tran P, Makarova AV, Chabes A, Burgers PM, Shcherbakova PV. 2017. Yeast DNA polymerase ζ maintains consistent activity and mutagenicity across a wide range of physiological dNTP concentrations. *Nucleic Acids Research* **45**: 1200–1218.
Koegl M, Uetz P. 2007. Improving yeast two-hybrid screening systems. *Briefings in functional genomics and proteomic*s. **6:** 302-312.
Lange SS, Takata K, Wood RD. 2011. DNA polymerases and cancer. *Nature Reviews Cancer* **11**: 96-110.
Lanzetta PA, Alvarez LJ, Reinach PS, Candia OA. 1979. An improved assay for nanomole amounts of inorganic phosphate. *Analytical Biochemistry* **100**: 95–97.

Lawrence CW, Das G, Christensen RB. 1985. REV7, a new gene concerned with UV mutagenesis in yeast. *Molecular & General Genetics* **200**: 80–85.
Lawrence CW, Nisson PE, Christensen RB.1985. UV and chemical mutagenesis in *rev7* mutants of yeast. *Molecular & General Genetics* **200**, 86–91.
Lejault P, Mitteaux J, Sperti FR, Monchaud D. 2021. How to untie G-quadruplex knots and why? *Cell Chemical Biology* **28**:436-455.
Leland BA, Chen AC, Zhao AY, Wharton RC, King MC. 2018. Rev7 and 53BP1/Crb2 prevent RecQ helicase-dependent hyper-resection of DNA double-strand breaks. *Elife* **7**: e33402.
Lemontt JF. 1971. Mutants of yeast defective in mutation induced by ultraviolet light. *Genetics* **68**: 21–33.
Liang L, Feng J, Zuo P, Yang J, Lu Y, Yin Y. 2020. Molecular basis for assembly of the shieldin complex and its implications for NHEJ. *Nature Communications* **11**: 1972.
Liang L, Feng J, Zuo P, Yang J, Lu Y, Yin Y. 2020. Molecular basis for assembly of the shieldin complex and its implications for NHEJ. *Nature Communications* **24**: 1972.
Ling JA, Frevert Z, Washington MT. 2022. Recent advances in understanding the structures of translesion synthesis DNA polymerases. *Genes (Basel)* **13**: 915.
Listovsky T, Sale JE. 2013. Sequestration of CDH1 by MAD2L2 prevents premature APC/C activation prior to anaphase onset. *The Journal of Cell Biology* **203**: 87–100.
Lobachev KS, Gordenin DA, Resnick MA. 2002. The Mre11 complex is required for repair of hairpin-capped double-strand breaks and prevention of chromosome rearrangements. *Cell* **108**, 183-193.
Ma JL, Kim EM, Haber JE, Lee SE. 2003. Yeast Mre11 and Rad1 proteins define a Ku-independent mechanism to repair double-strand breaks lacking overlapping end sequences. *Molecular and Cellular Biology* **23**, 8820–8828.
Mahmood T, Yang PC. 2012. Western Blot: Technique, theory, and trouble shooting. *North American journal of medical sciences* **4**: 429–434.
Maiorano D, El Etr J, Franchet C, Hoffmann JS. 2021. Translesion synthesis or repair by specialized DNA polymerases limits excessive genomic instability upon replication stress.

The International Journal of Molecular Sciences **22**: 3924.
Makarova AV, Burgers PM. 2015. Eukaryotic DNA polymerase ζ. *DNA Repair* **29**: 47–55.
Makarova AV, Stodola JL, Burgers PM. 2012. A four-subunit DNA polymerase zeta complex containing Pol delta accessory subunits is essential for PCNA-mediated mutagenesis. *Nucleic Acids Research* **40**: 11618–11626.
Malik R, Johnson RE, Prakash L, Prakash S, Ubarretxena-Belandia I, Aggarwal AK. 2022. Cryo-EM structure of translesion DNA synthesis polymerase ζ with a base pair mismatch. *Nature Communications* **13**: 1050.
Malik R, Kopylov M, Gomez-Llorente Y, Jain R, Johnson RE, Prakash L, Prakash S, Ubarretxena-Belandi I, Aggarwal AK. 2020. Structure and mechanism of B-family DNApolymerase ζ specialized for translesion DNA synthesis. *Nature Structural & Molecular Biology* **27**: 913–924.
Mirdita M, Schutze K, Moriwaki Y, Heo L, Ovchinnikov S, Steinegger M. 2022. ColabFold: making protein folding accessible to all. *Nature Methods* **19**:679–682.
Mirman Z, Lottersberger F, Takai H, Kibe T, Gong Y, Takai K, Bianchi A, Zimmermann M, Durocher D, de Lange T. 2018. 53BP1-RIF1-shieldin counteracts DSB resection through CST- and Polα-dependent fill-in. *Nature* **560**: 112–116.
Moore JK, Haber JE. 1996. Cell cycle and genetic requirements of two pathways of nonhomologous end-joining repair of double-strand breaks in *Saccharomyces cerevisiae*. *Molecular and Cellular Biology* **16**, 2164–2173.
Moreau S, Ferguson JR, Symington LS. 1999. The nuclease activity of Mre11 is required for meiosis but not for mating type switching, end joining, or telomere maintenance. *Molecular and Cellular Biology* **19**: 556–566.
Morrison A, Christensen RB, Alley J, Beck AK, Bernstine EG, Lemontt JF, Lawrence CW. 1989. *REV3*, a *Saccharomyces cerevisiae* gene whose function is required for induced mutagenesis, is predicted to encode a nonessential DNA polymerase. *The Journal of Bacteriology* **171**: 5659–5667.
Muniyappa K, Anuradha S, Byers B. 2000. Yeast meiosis-specific protein Hop1 binds to G4 DNA and promotes its formation. *Molecular and Cellular Biology* **20**: 1361–1369.
Muniyappa K, Kshirsagar R, Ghodke I. 2014. The HORMA domain: An evolutionarily conserved domain discovered in chromatin-associated proteins, has unanticipated diverse functions. *Gene* **545**: 194–197.
Nelson JR, Lawrence CW, Hinkle DC. 1996. Thymine-thymine dimer bypass by yeast DNA polymerase ζ. *Science* **272**: 1646–1649.
Noordermeer SM, Adam S, Setiaputra D, Barazas M, Pettitt SJ, Ling AK, Olivieri M, Álvarez-Quilón A, Moatti N, Zimmermann M, *et al*. 2018. The shieldin complex mediates 53BP1-dependent DNA repair. *Nature* **560**; 117–121.
Northam MR, Garg P, Baitin DM, Burgers PM, Shcherbakova PV. 2006. A novel function of DNA polymerase ζ regulated by PCNA. *The EMBO Journal* **25**: 4316–4325.
Oh J, Al-Zain A, Cannavo E, Cejka P, Symington LS. 2016. Xrs2 Dependent and independent functions of the Mre11-Rad50 complex. *Molecular Cell* **64**: 405-415.
Paeschke K, Bochman ML, Garcia PD, Cejka P, Friedman KL, Kowalczykowski SC, Zakian VA. 2013. Pif1 family helicases suppress genome instability at G-quadruplex motifs. *Nature* **497**: 458–462.
Paeschke K, Capra JA, Zakian VA. 2011. DNA replication through G-quadruplex motifs is promoted by the *Saccharomyces cerevisiae* Pif1 DNA helicase. *Cell* **145**: 678–691.
Paniagua I, Jacobs JJL. 2023. Freedom to err: The expanding cellular functions of translesion DNA polymerases. *Molecular Cell* **83(20)**: 3608–3621.
Paull TT, Gellert M. 1998. The 3' to 5' exonuclease activity of Mre11 facilitates repair of DNA double-strand breaks. *Molecular Cell* **1**: 969–979.
Paull TT. 2018. 20 Years of Mre11 biology: No end in sight. *Molecular Cell* **71**: 419–427.

Piano V, Alex A, Stege P, Maffini S, Stoppiello GA, Huis In 't Veld PJ, Vetter IR, Musacchio A. 2021. CDC20 assists its catalytic incorporation in the mitotic checkpoint complex. *Science* **371**, 67–71.

Pilzecker B, Buoninfante OA, Jacobs H. 2019. DNA damage tolerance in stem cells, ageing, mutagenesis, disease and cancer therapy. *Nucleic Acids Research* **47**: 7163-7181.

Prakash S, Johnson RE, Prakash L. 2005. Eukaryotic translesion synthesis DNA polymerases: specificity of structure and function. *Annual Review of Biochemistry* **74**: 317–353.

Pustovalova Y, Bezsonova I, Korzhnev DM. 2012. The C-terminal domain of human Rev1 contains independent binding sites for DNA polymerase η and Rev7 subunit of polymerase ζ. *FEBS Letters* **586**; 3051-3056.

Quah SK, von Borstel RC, Hastings PJ. 1980. The origin of spontaneous mutation in *Saccharomyces cerevisiae*. *Genetics* **96**: 819-839.

Rhodes D, Lipps HJ. 2015. G-quadruplexes and their regulatory roles in biology. *Nucleic Acids Research* **43**: 8627–8637.

Rizzo AA, Vassel FM, Chatterjee N, D'Souza S, Li Y, Hao B, Hemann MT, Walker GC, Korzhnev DM. 2018. Rev7 dimerization is important for assembly and function of the Rev1/Polζ translesion synthesis complex. *Proceedings of the National Academy of Sciences USA* **115**: E8191–E8200.

Rosenberg SC, Corbett KD. 2015. The multifaceted roles of the HORMA domain in cellular signaling. *The Journal of Cell Biology* **211**: 745–755.

Sambrook J, Russell DW. 2001. Molecular Cloning: A Laboratory Manual. *3: Cold Spring Harbor Laboratory, Cold Spring Harbor, New York*.

Sarangi P, Clairmont CS, Galli LD, Moreau LA, D'Andrea AD. 2020. p31^{comet} promotes homologous recombination by inactivating REV7 through the TRIP13 ATPase. *Proceedings of the National Academy of Sciences USA* **117**: 26795–26803.

Sarkies P, Murat P, Phillips LG, Patel KJ, Balasubramanian S, Sale JE. 2012. FANCJ coordinates two pathways that maintain epigenetic stability at G-quadruplex DNA. *Nucleic Acids Research* **40**: 1485-1498.

Sarkies P, Reams C, Simpson LJ, Sale JE. 2010. Epigenetic instability due to defective replication of structured DNA. *Molecular Cell* **40**: 703-713.

Sato K, Knipscheer P. 2023. G-quadruplex resolution: From molecular mechanisms to physiological relevance. *DNA Repair* **130**:103552.

Setiaputra D, Durocher D. 2019. Shieldin- the protector of DNA ends. *EMBO Reports* **20**, e47560.

Shibata A, Moiani D, Arvai AS, Perry J, Harding SM, Genois MM, Maity R, van Rossum-Fikkert S, Kertokalio A, Romoli F, *et al*. 2014. DNA double-strand break repair pathway choice is directed by distinct MRE11 nuclease activities. *Molecular Cell* **53**: 7–18.

Sonoda E, Okada T, Zhao GY, Tateishi S, Araki K, Yamaizumi M, Yagi T, Verkaik NS, van Gent DC, Takata M, Takeda S. 2003. Multiple roles of Rev3, the catalytic subunit of polzeta in maintaining genome stability in vertebrates. *The EMBO Journal* **22**: 3188–3197.

Spiegel J, Adhikari S, Balasubramanian S. 2020. The structure and function of DNA G-quadruplexes. *Trends in Chemistry* **2**: 123–136.

Stracker TH, Petrini JH. 2011. The MRE11 complex: starting from the ends. *Nature Reviews Molecular Cell Biology* **12**: 90–103.

Thakur M, Badugu S, Muniyappa K. 2020. UvrA and UvrC subunits of the *Mycobacterium tuberculosis* UvrABC excinuclease interact independently of UvrB and DNA. *FEBS Letters* **594**: 851–863.

Thakur M, Kumar MB, Muniyappa K. 2016. *Mycobacterium tuberculosis* UvrB Is a Robust DNA-Stimulated ATPase That Also Possesses Structure-Specific ATP-Dependent DNA Helicase Activity. *Biochemistry* **55**: 5865-5883.

Thakur M, Mohan D, Singh AK, Agarwal A, Gopal B, Muniyappa K. 2021. Novel insights

into ATP-stimulated cleavage of branched DNA and RNA substrates through structure-guided studies of the Holliday junction resolvase RuvX. *The Journal of Molecular Biology* **433**: 167014.

Tomida J, Takata KI, Bhetawal S, Person MD, Chao HP, Tang DG, Wood RD. 2018. FAM35A associates with REV7 and modulates DNA damage responses of normal and BRCA1-defective cells. *The EMBO Journal* **37**: e99543.

Trujillo KM, Sung P. 2001. DNA structure-specific nuclease activities in the *Saccharomyces cerevisiae* Rad50-Mre11 complex. *The Journal of Biological Chemistry* **276**, 35458-35464.

Tsubouchi H, Ogawa H. 1998. A novel mre11 mutation impairs processing of double-strand breaks of DNA during both mitosis and meiosis. *Molecular and Cellular Biology* **18**: 260–268.

Usui T, Ohta T, Oshiumi H, Tomizawa T, Ogawa H, Ogawa T. 1998. Complex formation and functional versatility of Mre11 of budding yeast in recombination. *Cell* **95**:705-16.

Vaisman A, Woodgate R. 2017. Translesion DNA polymerases in eukaryotes: what makes them tick? *Critical Reviews in Biochemistry and Molecular Biology* **52**: 274-303.

Varadi M, Anyango S, Deshpande M, Nair S, Natassia C, Yordanova G, *et al*. 2022. AlphaFold Protein Structure Database: Massively expanding the structural coverage of protein-sequence space with high-accuracy models. *Nucleic Acids Research* **50**: D439–D444.

You X, Nguyen AW, Jabaiah A, Sheff MA, Thorn KS, Daugherty PS. (2006) Intracellular protein interaction mapping with FRET hybrids. *Proceedings of the National Academy of Sciences USA* **103**: 18458-18463.

Wienken CJ, Baaske P, Rothbauer U, Braun D, Duhr S. 2010. Protein-binding assays in biological liquids using microscale thermophoresis. *Nature Communications* 2010; **1**: 100.

Xu G, Chapman JR, Brandsma I, Yuan J, Mistrik M, Bouwman P, Bartkova J, Gogola E, Warmerdam D, Barazas M, *et al*. 2015. *REV7* counteracts DNA double-strand break resection and affects PARP inhibition. *Nature* **521**: 541–544.

Yadav P, Kim N, Kumari M, Verma S, Sharma TK, Yadav V, Kumar A. 2021. G-quadruplex structures in bacteria: biological relevance and potential as an antimicrobial target. *The Journal of Bacteriology* **203**: e0057720.

Zhang X, Paull TT. 2005. The Mre11/Rad50/Xrs2 complex and non-homologous end-joining of incompatible ends in *S. cerevisiae*. *DNA Repair* **4**: 1281–1294.

Zhong X, Garg P, Stith CM, Nick McElhinny SA, Kissling E, Burgers PM, Kunkel TA. 2006. The fidelity of DNA synthesis by yeast DNA polymerase zeta alone and with accessory proteins. *Nucleic Acids Research* **34**: 4731–4742.

Zubarev RA, Makarov A. 2013. Orbitrap mass spectrometry. *Analytical Chemistry* **85,** 5288–5296.

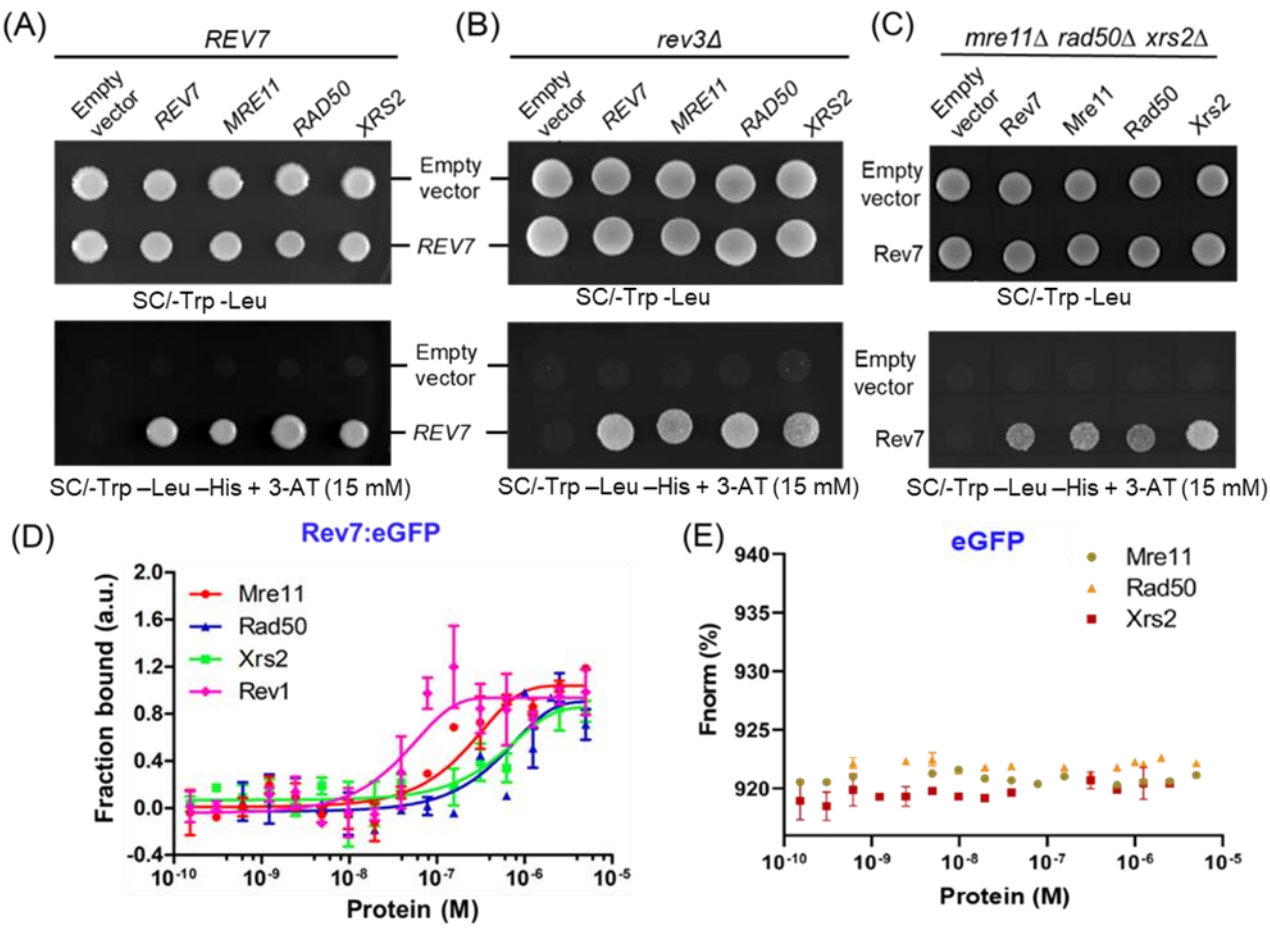

(F)

Target/Ligand	K_d values (μM)	Hill coefficient (n_H)
Rev7/ Mre11	0.23 ± 0.06	2.64 ± 1.80
Rev7/ Rad50	0.16 ± 0.07	1.31 ± 0.16
Rev7/Xrs2	0.56 ± 0.12	1.28 ± 0.70
Rev7/Rev1	0.11 ± 0.04	1.80 ± 0.0

Figure 1. Y2H screens suggest interaction between ScRev7 and the MRX subunits. The Y2H assay was performed in: (**A**) WT, (**B**) *rev3Δ* , and (**C**) *mre11Δ rad50Δ xrs2Δ* mutant strains. These strains were cotransformed with pairwise combinations of empty vector, bait (pGBKT7-*REV7*) and prey (pGADT7/*MRE11*, *RAD50*, *XRS2* or *REV7)* plasmids. Equal number of mid-log phase cells were spotted onto the SC/-Trp -Leu agar plates (upper panels) or SC/-Trp -Leu -His agar plates containing 3-AT (bottom panels). Cells were imaged after 48 h of growth at 30 °C. The images shown in panels (**A**), (**B**) and (**C**) are representative of three independent experiments. (**D**) and (**E**), normalized MST binding curves obtained for the titration of Mre11, Rad50, Xrs2 and Rev1 proteins against Rev7-eGFP or eGFP, respectively. Error bars indicate SEM, and data are representative of three independent experiments. (**F**) Quantitative parameters for interaction between ScRev7and Mre11, Rad50, Xrs2 or Rev1 proteins.

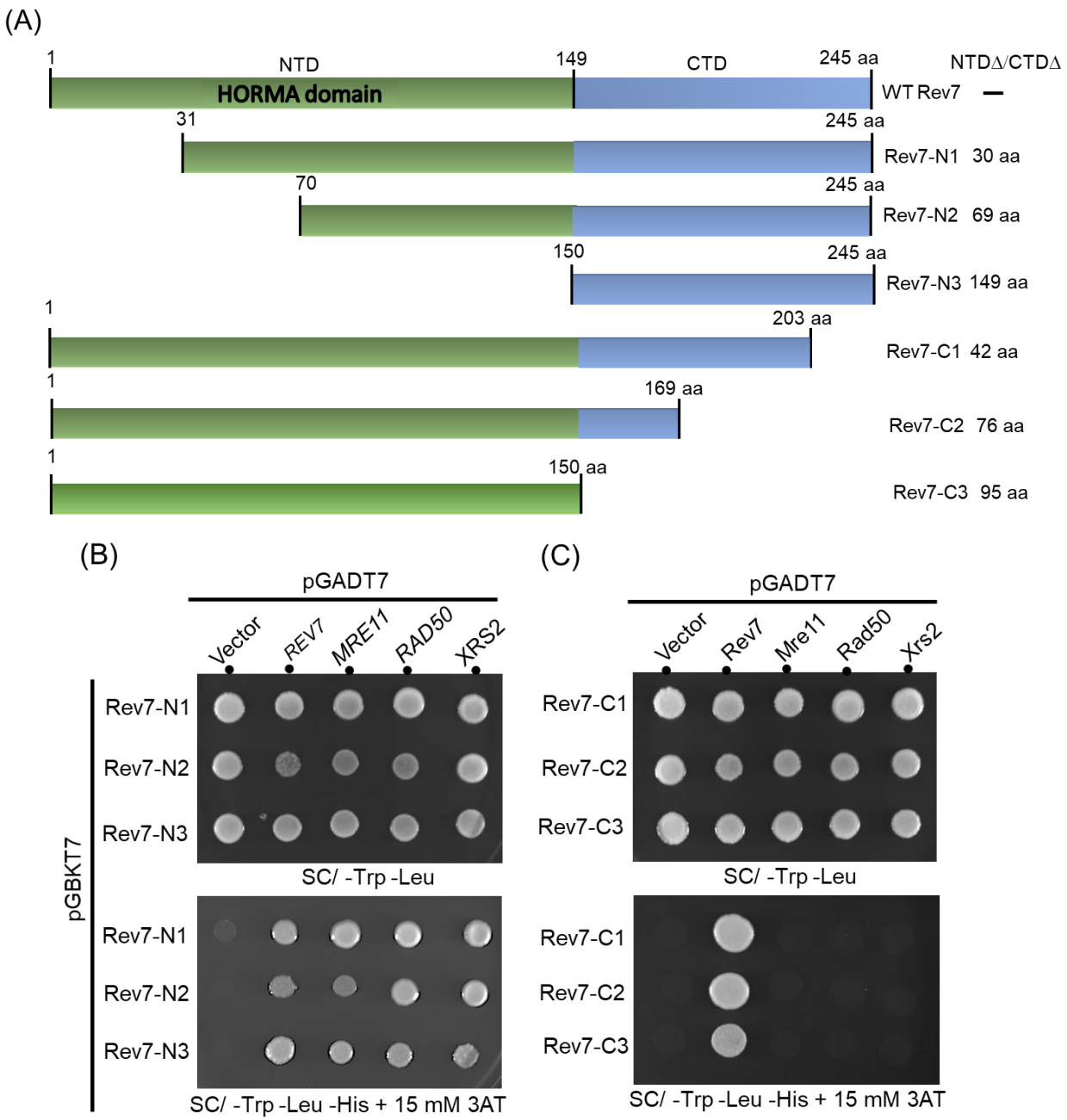

Figure 2. Deletion analysis revealed that the C-terminal 42 amino acids of ScRev7 are critical for its binding to the MRX subunits. (**A**) Schematic representation of the full- length and truncated ScRev7 variants. The truncated species lacking the indicated number of amino acids (aa) in the N-terminal domain (NTDΔ) or C-terminal domain (CTDΔ) is indicated on the right-hand side of the figure. (**B**) Representative images of spot assays of cells carrying pairwise combination of empty vector, bait and prey plasmids expressing N-terminally truncated species of Rev7 and full-length Rev7, Mre11, Rad50, Xrs2, respectively. (**C**) Same as panel (**B**), but with the bait plasmids encoding C-terminally truncated Rev7 variants. Cells were imaged after 48h of growth at 30 °C. Y2H assay was performed as described in the legend to *Figure 1*. Data are representative of three independent experiments.

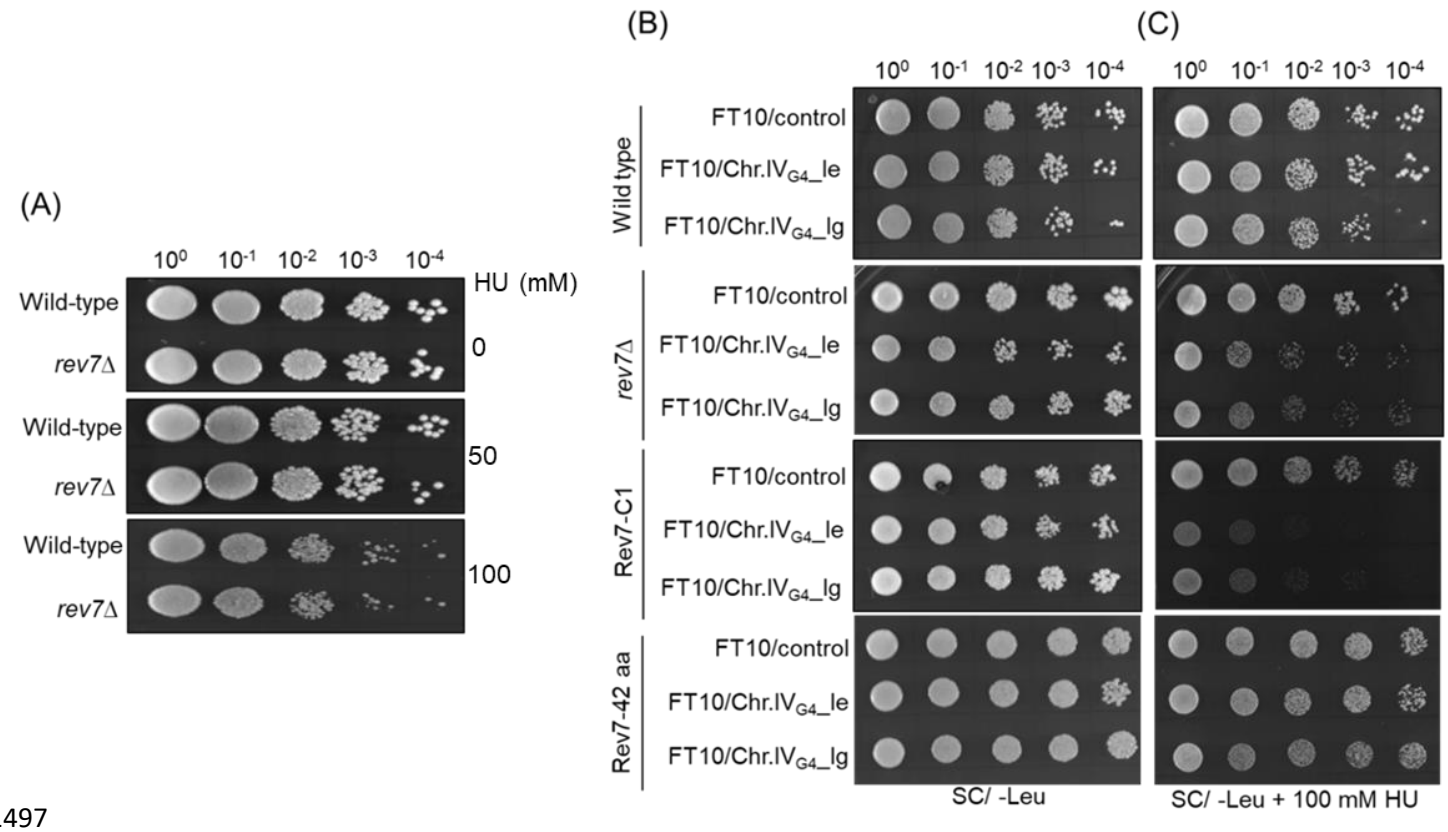

Figure 3. A 42-amino acid segment at the extreme C-terminus of ScRev7 renders cells resistant to the synergistic adverse effect of G-quadruplex DNA and HU. (**A**) *REV7* deletion does not affect HU sensitivity of *rev7Δ* cells. Representative images of YPD pates showing spot assay of WT and *rev7Δ* cells in the absence or presence of 50 or 100 mM HU. (**B**) Representative images of SC/-Leu agar plates showing spot assay of WT, *rev7Δ*, *rev7*-C1 or *rev7*-42 aa cells harboring the indicated plasmids carrying G-quadruplex capable sequences derived from chromosome IV (Chr.IV$_{G4}$). The cells were grown on SC/-Leu agar plates in the absence of HU. (**C**) Same as panel (**B**), but the growth medium contained 100 mM HU. For serial dilutions, each strain was grown in SC/-Leu medium, normalized to OD_{600} = 1.0, and serially diluted using yeast nitrogen base medium. Five µl aliquots from the serial dilutions were spotted onto the SC/-Leu agar plates with or without HU. FT10/Control plasmid lacks the G-quadruplex DNA insert. The abbreviations “le” and “lg” stand for leading and lagging strands, respectively. Cells were imaged after 4 days of growth at 30 °C. Data are representative of three independent experiments.

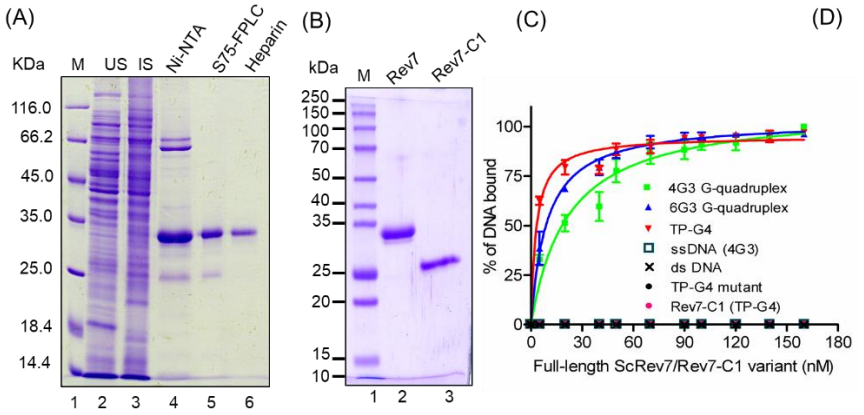

Substrate	K_d (nM)
ssDNA (Rev7)	ND
dsDNA (Rev7)	ND
4G3-G4 (Rev7)	18.26 ± 4.8
6G3-G4 (Rev7)	8.59 ± 1.43
TP-G4 (Rev7)	3.22 ± 0.36
TP-G4 mutant (Rev7)	ND
TP-G4 (Rev7-C1)	ND

Figure 4. ScRev7, but not the ScRev7-C1 variant, binds preferentially to G-quadruplex structures. (**A**) SDS-PAGE analysis of protein samples from different stages of ScRev7 purification. Lane 1: standard protein markers; 2, uninduced cell lysate (10 μg); 3, induced cell lysate (10 μg); 4, Ni^{2+}-NTA column eluate (3 μg); 5, Superdex S75 column eluate (1 μg); 6, eluate from heparin column (0.8 μg). (**B**) SDS-PAGE analysis of purified truncated ScRev7-C1 variant. Lane 1: standard protein markers. Lanes 2 and 3, purified full length ScRev7 and ScRev7-C1 variant. (**C**) Quantification of DNA binding specificities of ScRev7 or the variant ScRev7-C1. Each point in the graph represents mean values of three independent experiments. Four symbols [square (□), cross (x), black circle (•) and red circle (•)] overlap with each other, and are connected by a horizontal line along the x-axis. The best-fit curve was obtained by non-linear regression analysis by applying one-site binding model using Graph pad Prism (v 5.0). Error bars represent SEM of three independent experiments. (**D**) Apparent equilibrium dissociation constants (*Kd* values) for the binding of Rev7 or Rev7-C1 variant to the indicated DNA substrates. While G-quadruplex structures 4G3-G4 and 6G3-G4 contain four and six arrays of three guanine residues, respectively, TP-G4, contains one each of five, four and three arrays of guanine residues.

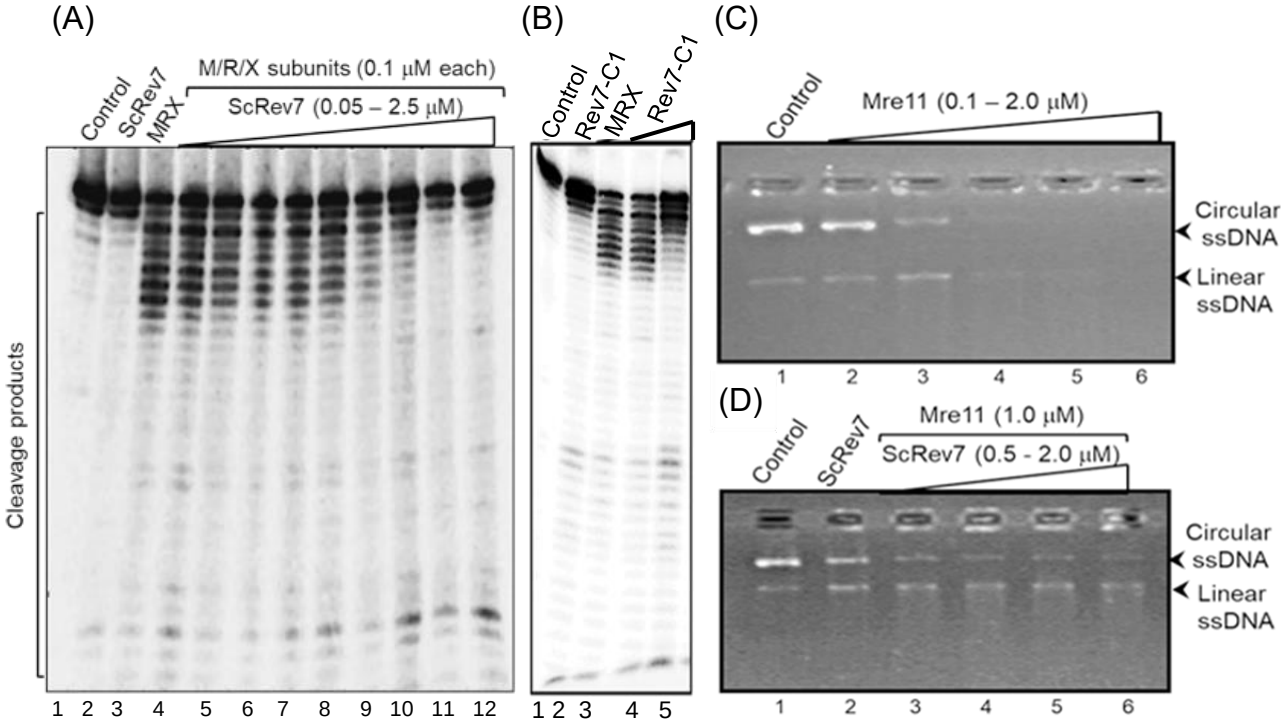

Figure 5. ScRev7 impedes both exo- and endonucleolytic activities of the MRX subunits. (**A**) A representative image showing the effect of ScRev7 on the exonuclease activity of MRX complex. Reaction mixtures containing 5 nM ^{32}P-labelled 60 bp dsDNA were incubated in the absence or presence of M/R/X subunits and various amounts of ScRev7. Lane 1, ^{32}P-labelled dsDNA. Lane 2, same as in lane 1, but with 2.5 μM ScRev7. Lane 3, same as in lane 1, but with M/R/X subunits (0.1 μM each). Lanes 4-12, same as in lane 3, but with 0.05, 0.1, 0.3, 0.5, 0.7, 1, 1.5, 2 and 2.5 μM of ScRev7, respectively. (**B**) A representative image showing the effect of Rev7-C1 variant on the exonuclease activity of the MRX complex. Assay was performed as in panel (**A**), but with ScRev7-C1 variant. Lane 1, ^{32}P-labelled dsDNA. Lane 2, same as in lane 1, but with 2.5 μM ScRev7-C1 variant. Lane 3, same as in lane 1, but with M/R/X subunits (0.1 μM each). Lanes 4-5, same as in lane 3, but with 1.5 and 3.0 μM of ScRev7-C1 variant, respectively. (**C**) A representative image showing Mre11 endonuclease activity on circular ssDNA. Reaction mixtures containing 100 ng M13 circular ssDNA were incubated without (lane 1) or with 0.1, 0.5, 1, 1.5 and 2 μM Mre11, respectively (lanes 2-6). (**D**) A representative image showing the effect of ScRev7 on Mre11 endonuclease activity by ScRev7. Reaction mixtures containing 1 μM Mre11 were pre-incubated with 0.5, 1.0 1.5 and 2 μM of ScRev7 (lanes 3-6 respectively), prior to the addition of 100 ng of M13 circular ssDNA. Lane 1, circular ssDNA alone. Lane 2, same as in lane 1, but with ScRev7. Increasing concentrations of the indicated protein is represented by open triangles at the top of the gel.

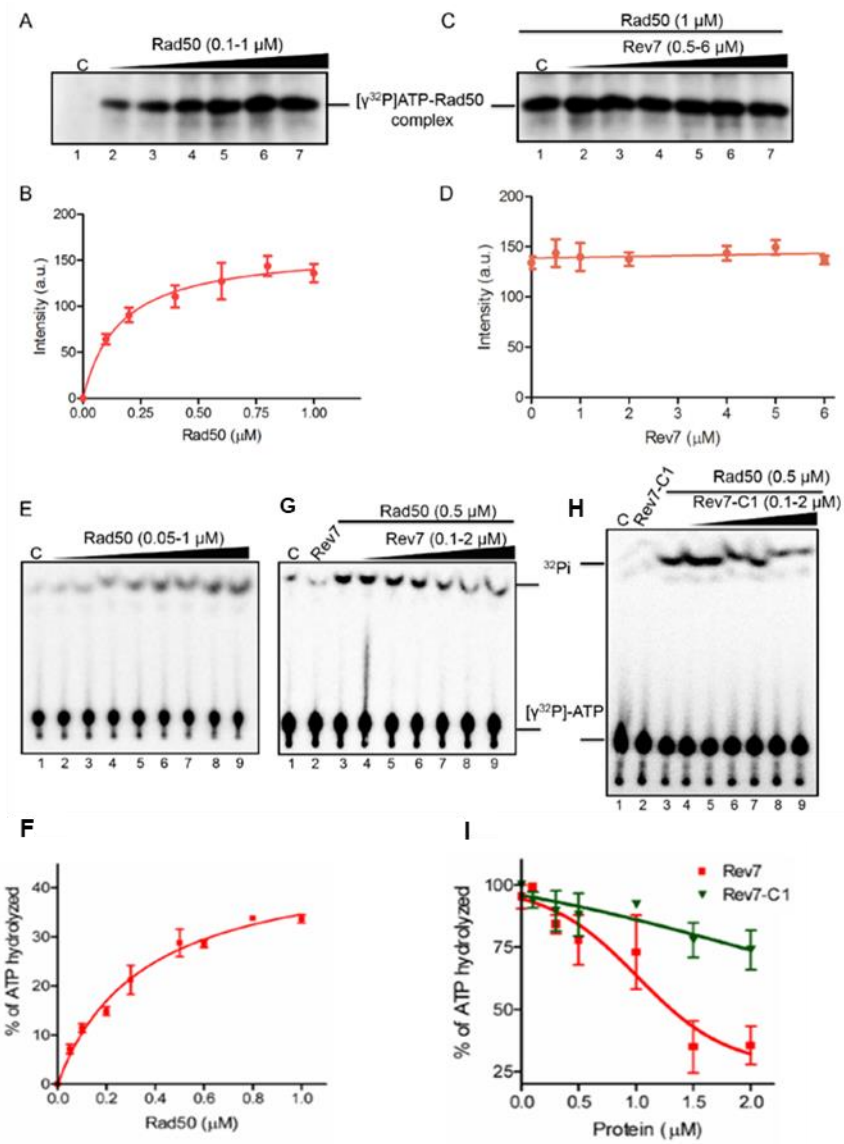

Figure 6. Rev7 inhibits the ATPase activity of Rad50 without impacting its ability to bind ATP. (**A**), Rad50 binds [γ-^{32}P]ATP in a dose-dependent manner. Lane 1, no protein. Lanes 2-7, reactions were performed with 0.1, 0.2, 0.4, 0.6, 0.8 and 1 μM of Rad50 and 400 pmol [γ-^{32}P]ATP. (**B**) Quantification of ATP binding by Rad50 as a function of its concentration. (**C**) ScRev7 does not affect the ability of Rad50 to bind ATP. Lane 1, Rad50 and 400 pmol [γ-^{32}P]ATP. Lanes 2-7, same as in lane 1, but with 0.5, 1, 2, 4, 5, and 6 μM of ScRev7, respectively. (**D**) Quantification of the effect of ScRev7 on ATP binding by Rad50. (**E**) ATPase activity of Rad50 as a function of its concentration. Reactions were performed in the absence (lane 1) or presence (lanes 2-9) of 0.05, 0.1, 0.2, 0.3, 0.5, 0.6, 0.8 and 1 μM of Rad50, respectively. (**F**) Quantification of Rad50 ATPase activity as a function of its concentration. (**G**) ScRev7 abrogates ATP hydrolysis catalyzed by Rad50. (**H**) ScRev7-C1 variant impedes ATP hydrolysis catalyzed by Rad50. In panels (G) and (H) lane 1 contained 400 pmol [γ-^{32}P]ATP; lane 2, same as in lane, but 2 μM ScRev7/ScRev7-C1 variant; lane 3, as in lane 1, but with 0.5 μM Rad50; lanes 4-9, as in lane 3, but with 0.5 μM Rad50 and 0.1, 0.3, 0.5, 1, 1.5 and 2 μM ScRev7/ScRev7-C1 variant, respectively. (**I**) Quantification of the inhibitory effect of ScRev7/ScRev7-C1 on ATP hydrolysis catalyzed by Rad50. The closed triangles on the top of gel images in panels (**A**), (**C**), (**E**), (**G**) and (**H**) represent increasing concentrations of Rad50, ScRev7 or ScRev7-C1. Error bars indicate SEM, and data are representative of three independent experiments.

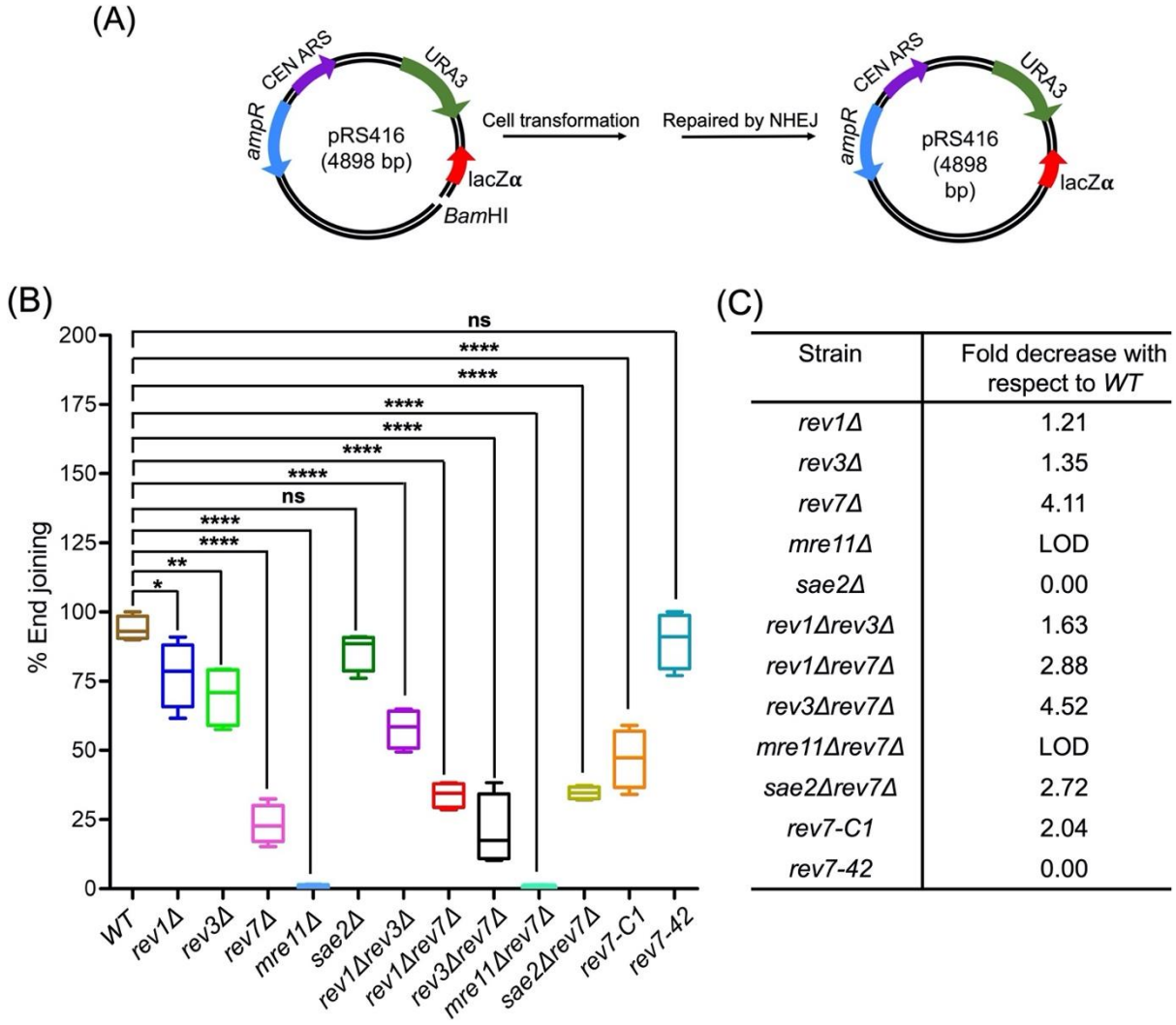

Strain	Fold decrease with respect to *WT*
rev1Δ	1.21
rev3Δ	1.35
rev7Δ	4.11
mre11Δ	LOD
sae2Δ	0.00
rev1Δrev3Δ	1.63
rev1Δrev7Δ	2.88
rev3Δrev7Δ	4.52
mre11Δrev7Δ	LOD
sae2Δrev7Δ	2.72
rev7-C1	2.04
rev7-42	0.00

Figure 7. *S. cerevisiae REV7* promotes NHEJ-mediated DSB repair. (**A**) Map of the NHEJ reporter plasmid and the experimental workflow. Sixty ng of uncut or linearized pRS416 plasmid DNA was transformed into the WT and indicated isogenic mutants carrying single or double deletions. Transformants were selected on SC medium lacking uracil. (**B**) Quantification of NHEJ efficiency relative to WT cells. (**C**) Quantification of fold decrease in the efficiency of NHEJ relative to the WT. The boxes represent mean; whiskers, minimum and maximum values. “LOD” denotes below the level of detection compared with the WT. The data are presented as the mean ± SEM of three independent experiments. n.s.: not significant, *$p < 0.05$, **$p < 0.005$, ****$p < 0.0001$ vs. control. The exact p-values are presented in *Supplementary Table S6*.

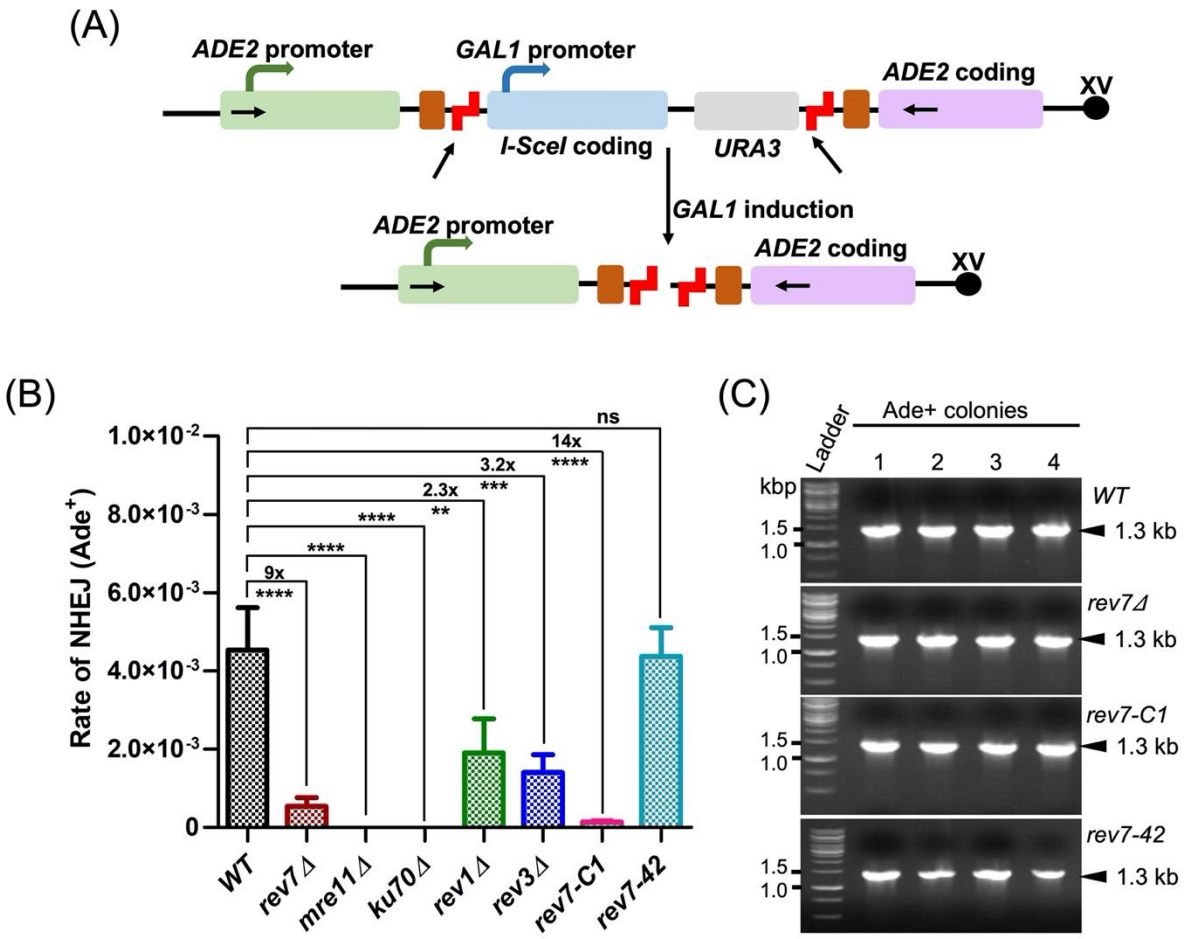

Figure 8. *S. cerevisiae REV7* facilitates chromosomal DSB repair *via* NHEJ pathway. (**A**) A schematic diagram showing the "suicide deletion" cassette at the *ADE2* locus of chromosome XV [redrawn from ref. Karathanasis and Wilson, 2002]. The arrows indicate the locations of PCR primers. Brown and staggered red boxes correspond to direct repeats and I-SceI cleavage sites, respectively. (**B**) Quantification of NHEJ efficiency in the WT and mutant strains. (**C**) Representative gel images of PCR-amplified DNA products from Ade^{2+} transformant cells. Data are means ± SEM from three independent experiments. n.s.: not significant, **p < 0.005, ***p < 0.001, ****p < 0.0001 vs. control, as assessed by one-way ANOVA Dunnett's multiple comparison test. The exact p-values are presented in *Supplementary Table S7*.

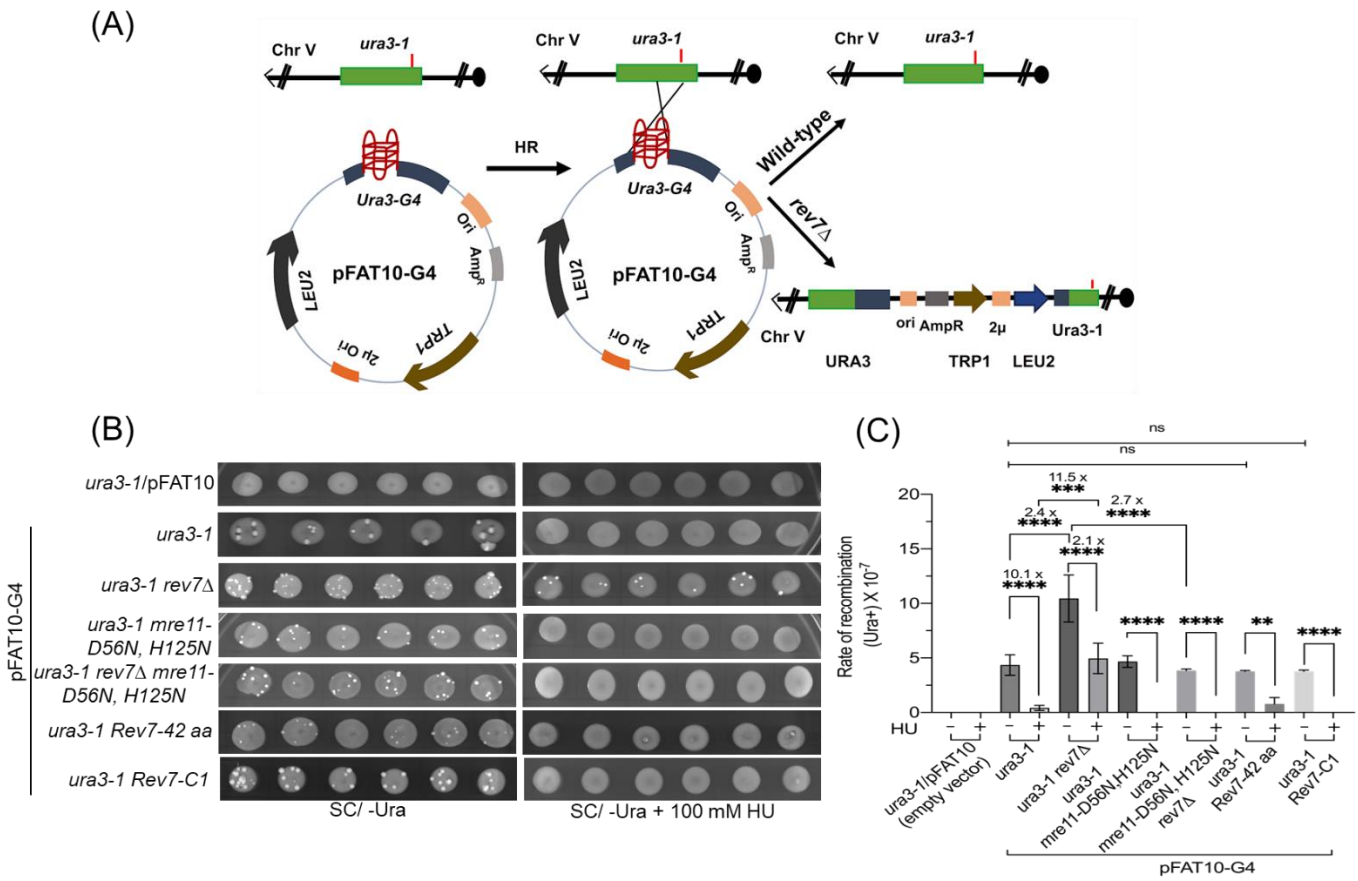

Figure 9. Deletion of *REV7* increases the frequency of mitotic HR. (**A**) Schematic representation of plasmid-chromosome recombination assay. The *ura3-1* and *ura3-G4* alleles are located on chromosome V and plasmid pFAT10-G4, respectively. Recombination between a plasmid borne *ura3-G4* allele and the chromosomal borne *ura3-1* allele would result in Ura+ prototrophs. (**B**) Representative images of Ura3^{+} papillae on SC/-Ura agar plates in the absence or presence of 100 mM HU. (**C**) Quantification of the rate of HR frequency in different strains. Data are presented as mean ± SD from three different experiments. ns, not significant, **p < 0.01, ***p < 0.001, ****p < 0.0001 vs. control, as assessed using one-way ANOVA and Tukey's post hoc test.

Supplemental figures and legends

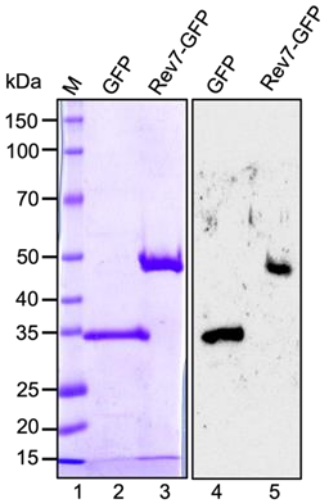

Figure 1—figure supplement 1. SDS-PAGE analysis of purified ScRev7-GFP.SDS-PAGE and western blot analysis of purified ScRev7-GFP. Lane 1, standard molecular weight markers; 2, purified GFP; 3, purified Rev7-GFP; Western blot analysis of (4) purified GFP and (5) Rev7-GFP, using mouse anti-GFP antibodies.

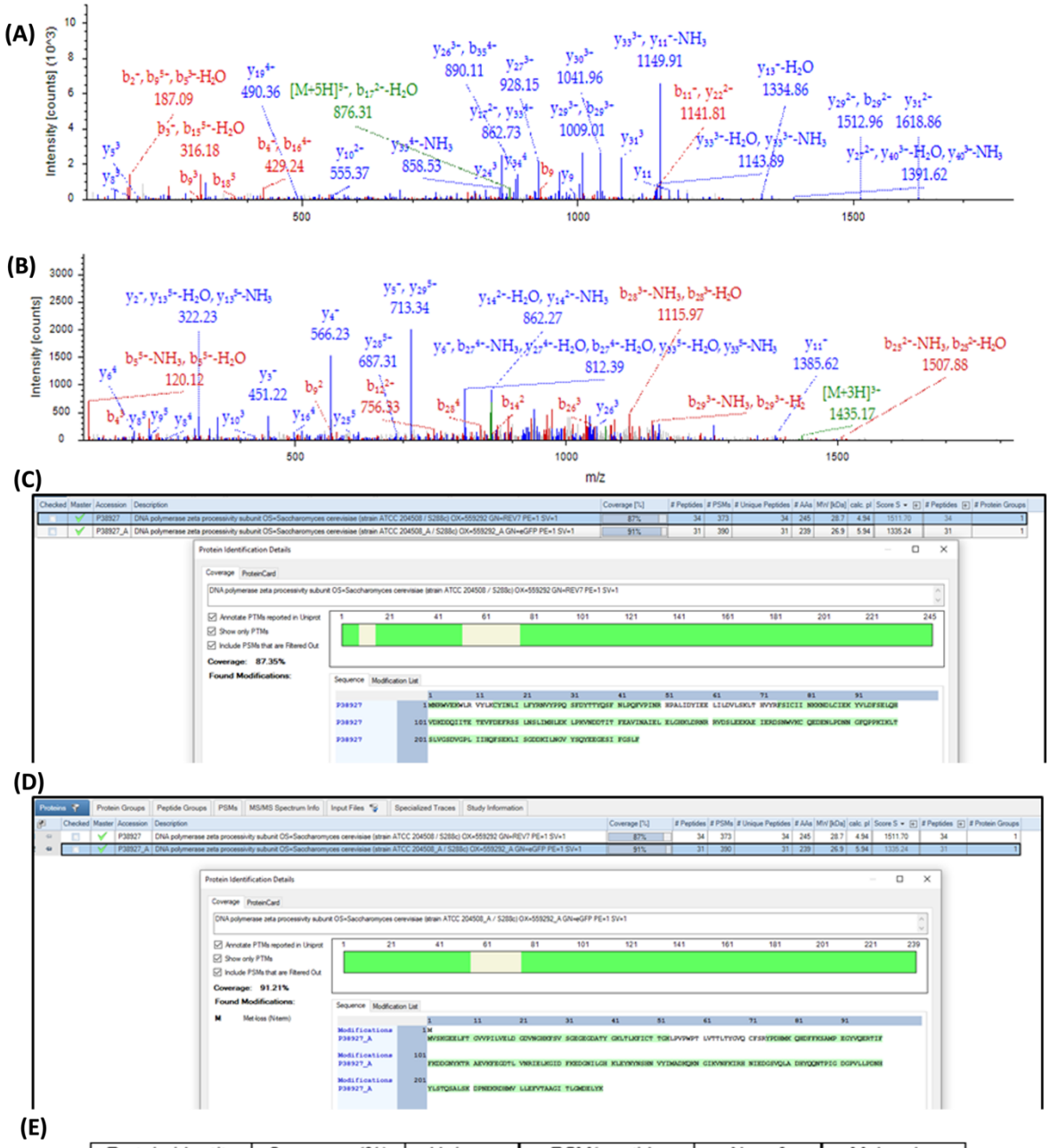

(E)

Protein identity	Coverage (%)	Unique peptides	PSM(peptide spectrum match)	No. of amino acids	Molecular weight (kDa)
Rev7	87	34	373	245	28.7
GFP	91	31	390	239	26.9

Figure 1—figure supplement 2. Representative spectra for unique peptides obtained after trypsin digestion of Rev7-GFP protein that match with (**A**) GFP sequence, (**B**) ScRev7 sequence. (**C**) Snapshot of sequence coverage (shown in green) obtained for Rev7 and (**D**) GFP. (**E**) Table summarizes data obtained for Orbitrap LC-MS performed using purified Rev7-GFP protein.

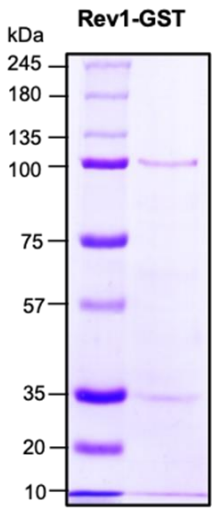

Figure 1—figure supplement 3. SDS-PAGE analysis of purified GST-tagged ScRev1. Lane 1, standard molecular weight markers; 2, purified GST tagged Rev1. The faster migrating band corresponds to ScRev7, which co-purifies with Rev1-GST (Acharya et al., 2005).

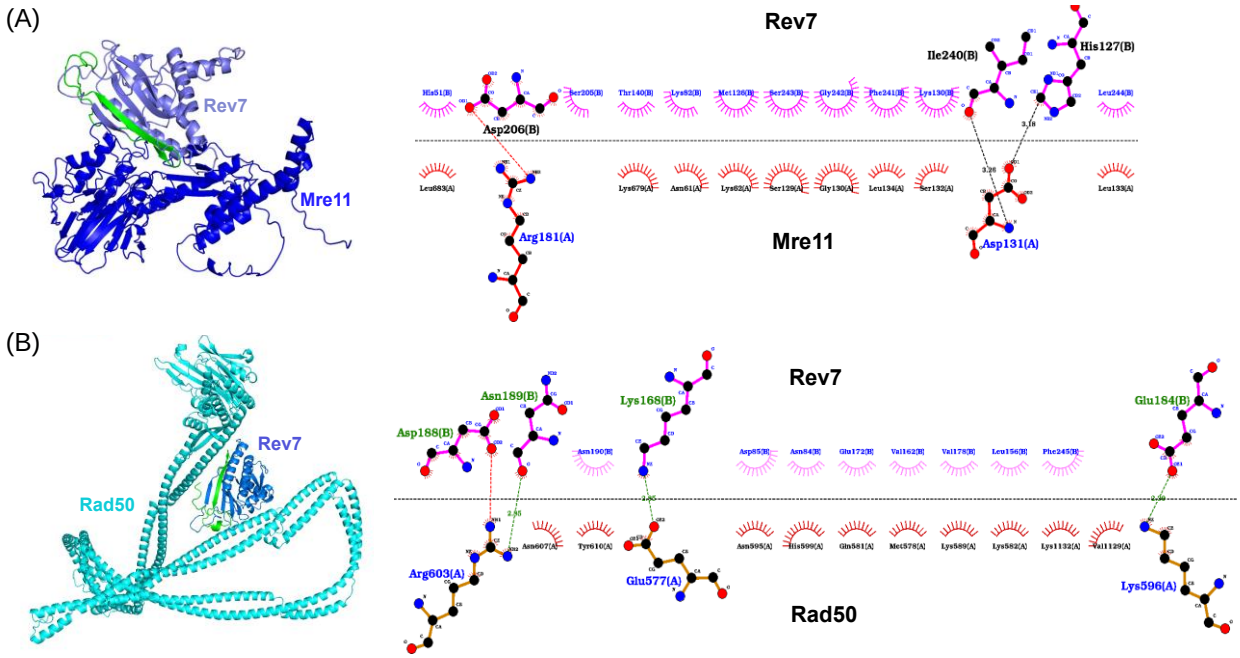

Figure 1—figure supplement 4. AlphaFold-Multimer generated models of Rev7-Mre11 and Rev7-Rad50 protein complexes. (A) Model of the Rev7-Mre11 heterodimer, Rev7, light blue, Mre11, deep blue. (B) Model of Rev7-Rad50 heterodimer, Rev7, light blue, Rad50, cyan. Alongside is the two-dimensional view of the corresponding protein-protein binding interface as generated by the LigPlot software. Numbers indicated on the dotted lines represent bond-lengths in Angstroms. The C-terminal safety belt region of Rev7 is coloured in green in both complexes. By convention, red, black and blue circles represent oxygen, carbon and nitrogen atoms respectively. The dashed line represents the interaction interface.

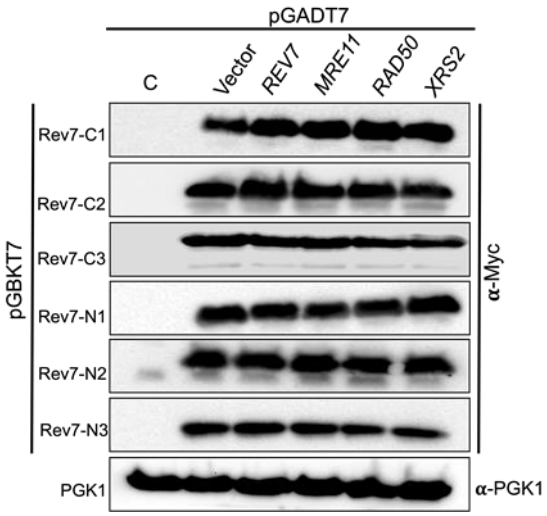

Figure 2—figure supplement 1. Western blot showing the abundance of N- and C-terminally truncated variants of Rev7. *S. cerevisiae* PJ69-4A cells were co-transformed with the indicated bait plasmid expressing c-Myc epitope tagged N- or C-terminally truncated variant of Rev7 (REV7-C1, REV7-C2, REV7-C3, REV7-N1, REV7-N2 or REV7-N3) with and a prey plasmid expressing *REV7, MRE11, RAD50* or XRS2. PGK-1 was used as the loading control and was probed with anti-PGK-1 antibodies. Sample loading was normalized to similar amounts by determining the protein concentration utilizing the dye-binding assay. Lane 'C' represents lysates from cells harboring empty bait and prey vectors.

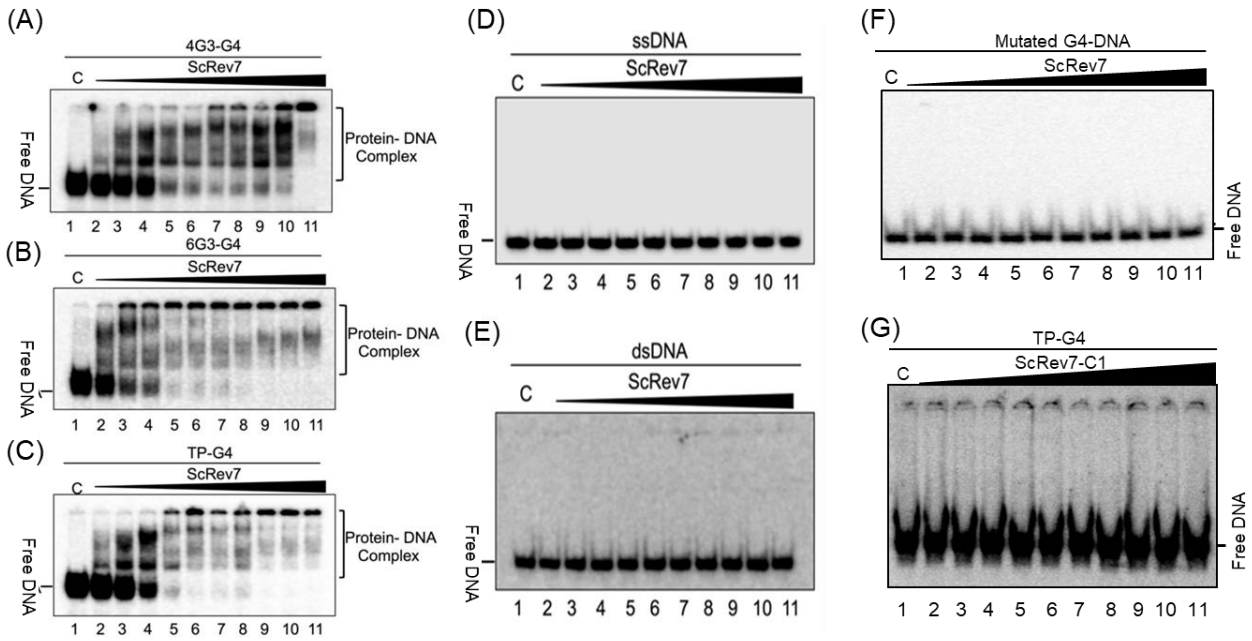

Figure 4—figure supplement 1. ScRev7 preferentially binds to G4 DNA, as opposed to ssDNA, dsDNA or mutated G4 DNA. Panels (**A-C**), Reaction mixtures containing 20 mM Tris-HCl (pH 6.8), 0.1 mM DTT, 0.2 μg/ml BSA, 5% glycerol, 0.5 nM of ^{32}P-labeled G-quadruplex structures with varying G4 motifs (indicated at the top of the gel) with varying concentrations of ScRev7. Lane 1 in all panels, the indicated DNA substrate without protein. Lanes 2-11, reactions performed with ScRev7 at 5, 20, 40, 50, 70, 90, 100, 120, 140 and 160 nM, respectively. Panels (**D-F**), similar to panels (**A-C**), but the reaction mixtures contained ^{32}P-labeled ssDNA, dsDNA or mutated G4 DNA (**G**), similar to panels (**D-F**), but reaction mixtures contained 25, 100, 200, 250, 350, 450, 500, 600, 650, 800 nM ScRev-C1 variant.

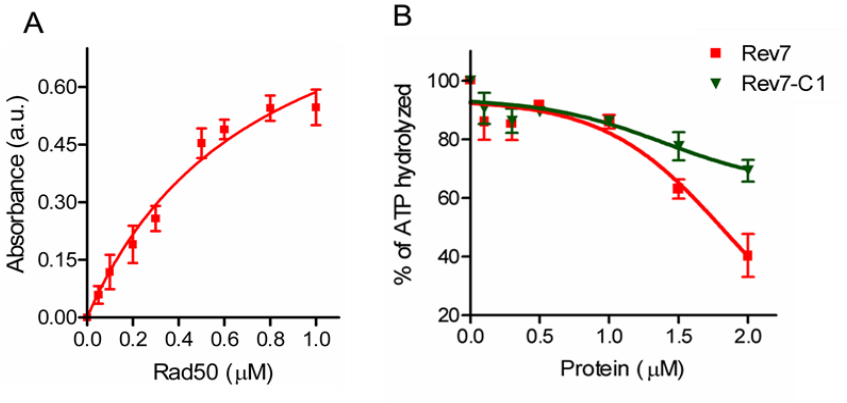

Figure 6—figure supplement 1. ScRev7 inhibits the ATPase activity of ScRad50. ATPase activity was measured using malachite green phosphate detection assay that quantifies the amount of Pi released upon ATP hydrolysis. (A) Increasing concentrations of ScRad50 (0, 0.05, 0.1, 0.2, 0.3, 0.5, 0.6, 0.8 and 1 μM) were incubated with reaction mixtures containing 20 mM Tris-HCl, pH 7.5, 50 mM KCl, 5% glycerol, 0.1 mM DTT, 0.2 mg/ml BSA, 150 μM ATP and 1 mM $MgCl_2$. Absorbance values were then monitored spectrophotometrically at 620 nm. (B) Same as (A), but fixed concentrations of ScRad50 (0.25 μM) were pre-incubated with increasing concentrations of ScRev7 or ScRev7-C1 (0, 0.1, 0.3, 0.5, 1, 1.5, 2 μM). The graphs were generated by non-linear regression analysis using GraphPad Prism (V. 5.0). Error bars represent standard deviation of data from two independent experiments.

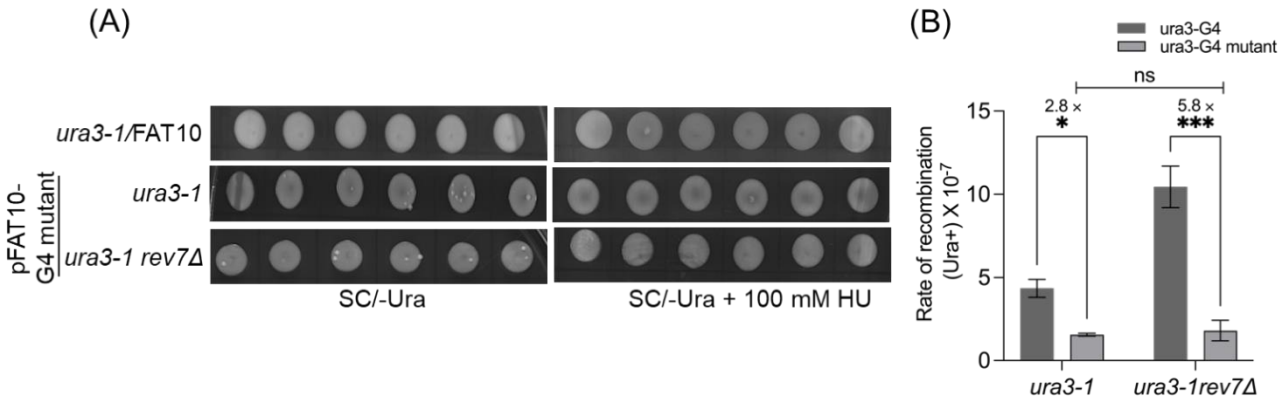

Figure 9—figure supplement 1. Mutation of G-quadruplex-forming sequences markedly attenuate the rate of HR frequency in *rev7Δ* cells. (**A**) Representative images showing Ura3^{+} papillae on SC/-Ura agar plates in the absence or presence of 100 mM HU. Cells were imaged after six days of growth at 30 °C. (**B**) Quantification of the rate of HR frequency in *ura3-1* and *ura3-1 rev7Δ* strains carrying plasmids with unmutated and mutated ura3-G4 inserts. Data are presented as mean ± SD from three different experiments. n.s., not significant, *p<0.05, and ***p < 0.001 vs. control, as assessed using two-way ANOVA and Sidaks multiple comparison test.

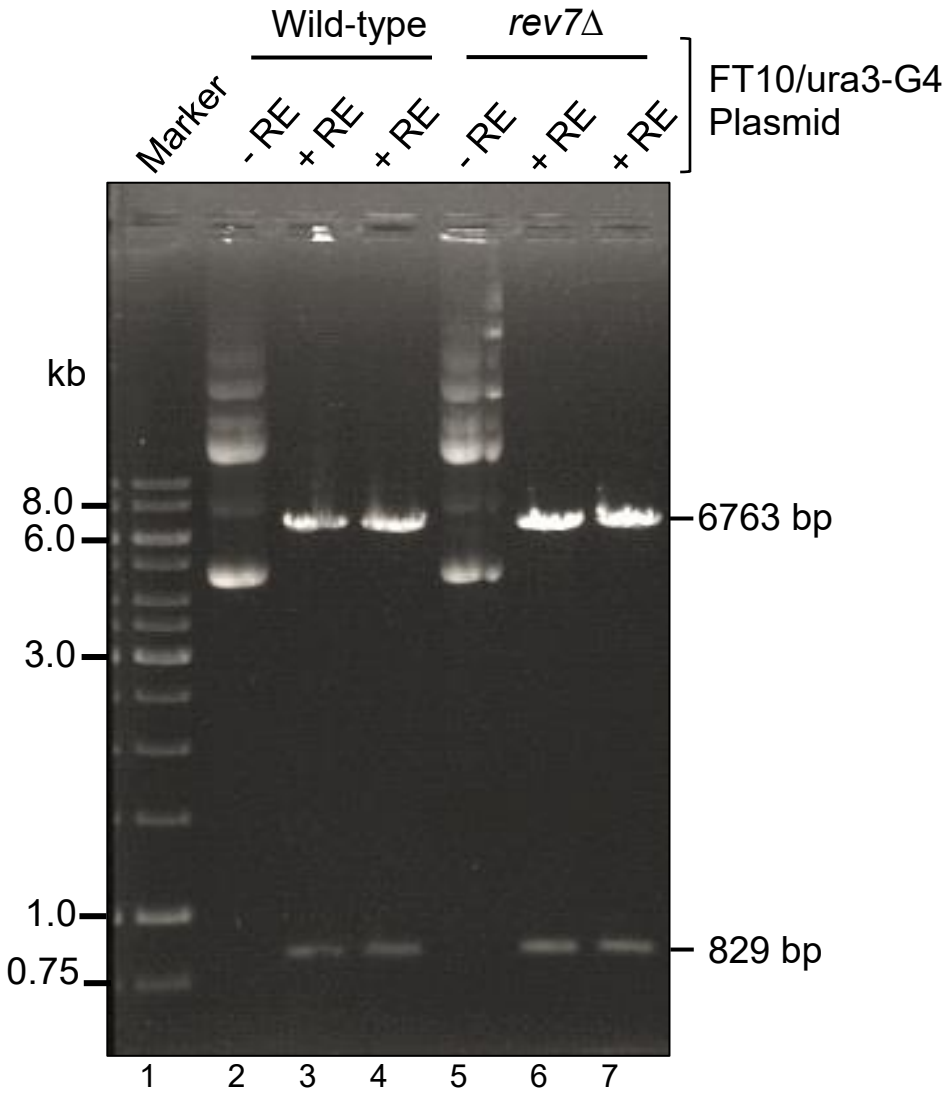

Figure 9—figure supplement 2. G-quadruplex capable sequences are stable in *rev7Δ* cells during the HR assay. Total plasmid pFAT10-G4 DNA was isolated from from cultures of WT and *rev7*Δ cells. Samples of undigested and BamHI and Sph1 digested plasmid pFAT10-G4 DNA were analyzed by electrophoresis on a 0.6 % agarose gel and visualized after staining with ethidium bromide. Lane1: DNA marker; 2 and 5, represent undigested plasmid DNA from the WT and *rev7*Δ cells respectively. Lanes 3 and 4, plasmid pFAT10-G4 DNA from the WT cells digested by BamHI and Sph1; 6 and 7, same as lane 3 and 5, but plasmid isolated from *rev7*Δ cells. + RE and –RE indicate DNA digested by BamHI and Sph1 and undigested plasmid DNA respectively.

Supplementary Tables

Table S1. Inter-atomic distances and confidence parameters of amino acid residues mediating Rev7-Mre11 interactions.

Mre11 (position of amino acid residue)	Rev7 (position of amino acid residue)	Distance (Å)	Mre11-residue	Rev7-residue	Mre11-pLDDT	Rev7-pLDDT
A_0181	B_0206	0.73	ARG	ASP	74.44	65.25
A_0062	B_0126	1.14	LYS	MET	77.81	71.25
A_0130	B_0242	1.27	GLY	GLY	42.81	20.97
A_0134	B_0241	1.36	LEU	PHE	72.12	22.19
A_0131	B_0242	1.38	ASP	GLY	42.41	20.97
A_0132	B_0241	1.86	SER	PHE	51.47	22.19
A_0130	B_0243	2.16	GLY	SER	42.81	20.88
A_0130	B_0241	2.23	GLY	PHE	42.81	22.19
A_0131	B_0241	2.23	ASP	PHE	42.41	22.19
A_0679	B_0082	2.24	LYS	LYS	26.53	81.81
A_0131	B_0240	2.52	ASP	ILE	42.41	26.36
A_0130	B_0130	2.74	GLY	LYS	42.81	72.25
A_0181	B_0207	2.77	ARG	VAL	74.44	63.84

Residues highlighted in green are present in the C-terminal safety-belt region of Rev7 protein.

Table S2. Inter-atomic distances and confidence parameters of amino acid residues mediating Rev7-Rad50 interactions

Rad50 (position of amino acid residues)	Rev7 (positions of amino acid residues)	Distance (Å)	Rad50-residue	Rev7-residue	Rad50-pLDDT	Rev7-pLDDT
A_0603	B_0188	1.26	ARG	ASP	73.56	51.81
A_0582	B_0156	1.45	LYS	LEU	73	69
A_0599	B_0084	1.88	HIS	ASN	73.56	68.56
A_0596	B_0184	2.3	LYS	GLU	75.75	62.81
A_1132	B_0245	2.5	LYS	PHE	81	18.19
A_0581	B_0172	2.58	GLN	GLU	72.12	80.44
A_1129	B_0245	2.6	VAL	PHE	79	18.19
A_0599	B_0085	2.78	HIS	ASP	73.56	74.62
A_0577	B_0168	2.85	GLU	LYS	71.31	77.94
A_0603	B_0189	2.85	ARG	ASN	73.56	46.66

Residues highlighted in green are present in the C-terminal safety-belt region of Rev7 protein.

Table S3. The exact p-values for Figure 7B. The p-values were obtained by comparing the percentage of non-homologous end-joining observed for the indicated single- or double-gene deletions versus either the wild-type (WT) or *rev7Δ* strain, using non-parametric one-way ANOVA Dunnett test.

Reference strain	**Strain**	**p-values**
WT	*rev1Δ*	0.0461
	rev3Δ	0.0011
	rev7Δ	<0.0001
	mre11Δ	<0.0001
	sae2Δ	0.7111
	rev1Δ rev3Δ	<0.0001
	rev1Δ rev7Δ	<0.0001
	rev3Δ rev7Δ	<0.0001
	mre11Δ rev7Δ	<0.0001
	sae2Δ rev7Δ	<0.0001
	rev7-C1	<0.0001
	rev7-42	0.9910
rev7Δ	*rev1Δ rev7Δ*	0.2731
	rev3Δ rev7Δ	0.9958
	mre11Δ rev7Δ	0.0029
	sae2Δ rev7Δ	0.2220
	rev7-C1	0.0022
	rev7-42	<0.0001

Table S4. The exact p-values for Figure 8B. The p-values were obtained by comparing the percentage of non-homologous end-joining observed for the indicated single- or double-gene deletions versus either the wild-type (WT) or *rev7Δ* strain, using non-parametric one-way ANOVA Dunnett test.

Reference strain	Strain	p-values
WT	*rev7Δ*	<0.0001
	mre11Δ	<0.0001
	ku70Δ	<0.0001
	rev1Δ	0.0046
	rev3Δ	0.0009
	rev7-C1	<0.0001
	rev7-42	0.369
rev7Δ	*rev7-C1*	0.3664
	rev7-42	0.0002

Table S5. *S. cerevisiae* strains used in this study.

Strain	Genotype	Source
W1588-4C	*MATa ura3-1 trp1-1 leu2-3 112 his3-11 15 ade2-1 can1-100 ybp1-1 RAD5*$^{+}$	Paeschke *et al*., 2011
KP013	*MATa ura3-1 trp1-1 leu2-3 112 his3-11 15 ade2-1 can1-100 ybp1-1 RAD5*$^{+}$ *bar1Δ::HIS3*	Paeschke *et al*., 2011
KMY017	*MATa ura3-1 trp1-1 leu2-3 112 his3-11 15 ade2-1 can1-100 ybp1-1 RAD5*$^{+}$ *bar1Δ::HIS3 rev7Δ:: kanMX4*	This Study
KMY042	*MATa ura3-1 trp1-1 leu2-3 112 his3-11 15 ade2-1 can1-100 ybp1-1 RAD5*$^{+}$ *bar1Δ::HIS3 rev1Δ:: hphNT1*	This Study
KMY061	*MATa ura3-1 trp1-1 leu2-3 112 his3-11 15 ade2-1 can1-100 ybp1-1 RAD5*$^{+}$ *bar1Δ::HIS3 rev3Δ::KanMX4*	This Study
KMY018	*MATa ura3-1 trp1-1 leu2-3 112 his3-11 15 ade2-1 can1-100ybp1-1 RAD5*$^{+}$ *bar1Δ::HIS3 mre11Δ:: hphNT1*	This Study
KMY141	*MATa ura3-1 trp1-1 leu2-3 112 his3-11 15 ade2-1 can1-100 ybp1-1 RAD5*$^{+}$ *bar1Δ::HIS3 rev7Δ::rev7-C1 (203-245 aaΔ)-9MYC-hphNT1*	This Study
KMY143	*MATa ura3-1 trp1-1 leu2-3 112 his3-11 15 ade2-1 can1-100 ybp1-1 RAD5*$^{+}$ *bar1Δ::HIS3 rev7Δ::rev7-42 (1-203 aaΔ)-3MYC-KANMX4*	This Study
LSY1375	*MATa ura3-1 trp1-1 leu2-3 112 his3-11 15 ade2-1 can1-100 ybp1-1 RAD5*$^{+}$ *mre11-D56N, H125N*	Krogh *et al*., 2005
LSY1091	*MATa ura3-1 trp1-1 leu2-3 112 his3-11 15 ade2-1 can1-100 ybp1-1 RAD5*$^{+}$ *sae2Δ:: kanMX6*	Krogh *et al*., 2005
KMY058	*MATa ura3-1 trp1-1 leu2-3 112 his3-11 15 ade2-1 can1-100 ybp1-1 RAD5*$^{+}$ *bar1Δ::HIS3 rev1Δ:: hphNT1 rev3Δ::KanMX4*	This Study
KMY059	*MATa ura3-1 trp1-1 leu2-3 112 his3-11 15 ade2-1 can1-100 ybp1-1 RAD5*$^{+}$ *bar1Δ::HIS3 rev7Δ:: kanMX4 rev3Δ:: hphNT1*	This Study
KMY048	*MATa ura3-1 trp1-1 leu2-3 112 his3-11 15 ade2-1 can1-100 ybp1-1 RAD5*$^{+}$ *bar1Δ::HIS3 rev1Δ:: hphNT1 rev7Δ:: kanMX4*	This Study
KMY050	*MATa ura3-1 trp1-1 leu2-3 112 his3-11 15 ade2-1 can1-100 ybp1-1 RAD5*$^{+}$ *rev7Δ:: kanMX4 mre11Δ:: hphNT1*	This Study
KMY053	*MATa ura3-1 trp1-1 leu2-3 112 his3-11 15 ade2-1 can1-100 ybp1-1 RAD5*$^{+}$ *mre11-D56N, H125N rev7Δ:: kanMX4*	This Study
KMY060	*MATa ura3-1 trp1-1 leu2-3 112 his3-11 15 ade2-1 can1-100 ybp1-1 RAD5*$^{+}$ *sae2Δ:: kanMX6 rev7Δ:: hphNT1*	This Study
KP038	*MATa ura3–52 lys2–801 ade2–101 trp1-Δ63 his1-*	Paeschke *et al*.,

	Δ200 leu2-Δ1 pif1-m2	2011
YW714	*MATα ade2::SD2-::URA3 his31 leu20 ura30*	Karathanasis and Wilson, 2002
KMY136	*MATα ade2::SD2-::URA3 his31 leu20 ura30 rev7Δ::hphNT1*	This Study
KMY137	*MATα ade2::SD2-::URA3 his31 leu20 ura30 mre11Δ::hphNT1*	This Study
KMY144	*MATα ade2::SD2-::URA3 his31 leu20 ura30 rev1Δ::hphNT1*	This Study
KMY145	*MATα ade2::SD2-::URA3 his31 leu20 ura30 rev3Δ::hphNT1*	This Study
KMY146	*MATα ade2::SD2-::URA3 his31 leu20 ura30 rev7Δ::REV7-C1 (203-245 aaΔ)-9MYC-hphNT1*	This Study
KMY147	*MATα ade2::SD2-::URA3 his31 leu20. ura30 rev7Δ::REV7-42 (1-203 aaΔ)-3MYC-KANMX4*	This Study
PJ69-4A	*MATa trpl-901 leu2-3,112 ura3-52 his3-200 ga14Δ ga180Δ LYS2::GALI-HIS3 GAL2-ADE2 met2::GAL7-lacZ*	James *et al*., 1996
KMY023	*MATa trpl-901 leu2-3,112 ura3-52 his3-200 ga14Δ ga180Δ LYS2::GALI-HIS3 GAL2-ADE2 met2::GAL7-lacZ rev3Δ:: hphNT1*	This Study
KMY139	*MATa trpl-901 leu2-3,112 ura3-52 his3-200 ga14Δ ga180Δ LYS2::GALI-HIS3 GAL2-ADE2 met2::GAL7-lacZ mre11Δ::KANMX4 rad50Δ::URA3 xrs2Δ::HphNT1*	This Study
BJ5464	MATα ura3-52 trp1 leu2-Δ1 his3-Δ200 pep4::HIS3 prb1-Δ1.6R can1 GAL	Johnson *et al*., 2006

Table S6. Sequences of primers

Primer names	**Sequence**	**Plasmid DNA/primers**
OSB01-FP	5'GC**GGATCC**ATGAATAGATGGGTAGAGAAGTG3'	pET28a_ScREV7, pET28a_ScREV7-C1
OSB02-RP	5' GC**AAGCTT**TTCTTCAAATTTCATTTTTGCAC3'	pET28a_ScREV7
OSB03-FP	5' **CATATG**ATGAATAGATGGGTAGAGAAGTG3'	pGBKT7_ScREV7, pGADT7_ScREV7
OSB04-RP	5' **GGATCC**TTCTTCAAATTTCATTTTTGCAC3'	pGBKT7_ScREV7, pGADT7_ScREV7
OSB05-FP	5'ATGCCT**CATATG**ATGGACTATCCTGATCCAGACACACAATAAGG3'	pGADT7_ScMRE11
MRE11_RP	5'ATGCCT**GAATTC**CTATTTTCTTTTCTTAGGAAGGAGGACTTCC3'	pGADT7_ScMRE11
OSB11-FP	5'ATCCAAGAAGAAAAAAAAAATAGTAATCGTTGCGTCAGCTTTATGCGTACGCTGCAGGTCGAC3'	REV7 Knockout

OSB12-RP	5’ACATTTAATTTTAATTCCATTCTTCAAATTTCATTTTTGCACTTAATCGATGAATTCGAGCTCG 3’	REV7 Knockout
OSB13-FP	5’ATATGCATATACGTCTACACTAC3’	REV7 Knockout
OSB14-RP	5’CTGCAGCGAGGAGCCGTAAT3’ (KANB)	REV7 Knockout
OSB33-FP	5’CGC**GGATCC**ATGAGCGCTATCTATAAATTATC3’	pESUMO_ScRAD50
OSB34-RP	5’CCG**CTCGAG**TCAATAAGTGACTCTGTTAATATC3’	pESUMO_ScRAD50 & pGADT7_ScRAD50
OSB35-FP	5’ CCG**GAATTC**ATGAGCGCTATCTATAAATTATC3’	pGADT7_ScRAD50
OSB36-FP	5’ GGAATTC**CATATG**ATGTGGGTAGTACGATACCAG3’	pGADT7_ScXRS2
OSB37-RP	5’ CG**GGATCC**TTATCCTTTTCTTCTTTTGAA3’	pGADT7_ScXRS2
OSB52-FP	5’ATTGACGCAAGTTGTACCTGCTCAGATCCGATAAAACTCGACTATGCGTACGCTGCAGGTCGAC3’	MRE11 Knockout
OSB53-RP	5’TGGTTATAAATAGGATATAATATAATATAGGGATCAAGTACAACTAATCGATGAATTCGAGCTCG3’	MRE11 Knockout
OSB54-FP	5’AAGGCATCTACAAATCTCATTG3’	MRE11 Knockout
OSB133-FP	5’AGGCAAAAATCACAAATTGAGTGGGTCGATATTAACAGAGTCACTTATCGTACGCTGCAGGTCGAC3’	RAD50 Knockout
OSB075-RP	5’TAATTAATCAATCAAAGTCTATCCCTTCGTAGATATTATGGGGTCTTTATCGATGAATTCGAGCTCG3’	RAD50 Knockout
OSB076-RP	5’TCCTTGGTTAACAACGGTG3’	RAD50 Knockout
OSB134-FP	5’ACGACGACGATGACGACGGTCCGAAGTTTACGTTCAAAAGAAGAAAAGGACGTACGCTGCAGGTCGAC3’	XRS2 Knockout
OSB078-RP	5’TGCAAAATATAATTTAATGAAATTGGAAATACTCGGAAAATTTATCATTAATCGATGAATTCGAGCTCG3’	XRS2 Knockout
OSB079-RP	5’TTGGAGTATTCAAAGAGGCTAC3’	XRS2 Knockout
OSB55-FP	5’TTCTCAAAATAAATCGATACTGCATTTCTAGGCATATCCAGCGATGCGTACGCTGCAGGTCGAC3’	REV1 Knockout
OSB56-FP	5’AACTGCGTGTTTACTGTATGCTGAAATGTTTTTTTTTTTTTAATTCAATCGATGAATTCGAGCTCG3’	REV1 Knockout
OSB57-FP	5’TTTACACAGACCAAGACGG3’	REV1 Knockout
OSB58-FP	5’TCAATACAAAACTACAAGTTGTGGCGAAATAAAATGTTTGGAAATGCGTACGCTGCAGGTCGAC3’	REV3 Knockout
OSB59-RP	5’ACAAATAACTACTCATCATTTTGCGAGACATATCTGTGTCTAGATTAATCGATGAATTCGAGCTCG3'	REV3 Knockout
OSB60-FP	5’ATCCCTGTGGTCTCCTACC3’	REV3 Knockout
OSB116-FP	5’ATCCAAGAAGAAAAAAAAAATAGTAATCGTTGCGTCAGCTTTATGAATAGATGGGTAGAGAAGTG3’	*rev7-c1* truncation (rev7-c1-9MYC-hphNT1)
OSB117-RP	5’GTCGACCTGCAGCGTACGGACTAAAGAAGTGAGTTTTATTTTAGG3’	*rev7-c1* truncation (rev7-c1-9MYC-hphNT1)
OSB118-FP	5’CCTAAAATAAAACTCACTTCTTTAGTCCGTACGCTGCAGGTCGAC3’	*rev7-c1* truncation (rev7-c1-9MYC-hphNT1)
OSB070-RP	5’TACTTAGAGACATTTAATTTTAATTCCATTCTTCAAATTTCATTTTTGCACTTAATCGATGAATTCGAGCT	*rev7-c1* truncation (rev7-c1-9MYC-

	CG3’	hphNT1)
OSB122-FP	5’ATCCAAGAAGAAAAAAAAAATAGTAATCGTTGCG TCAGCTTTATGGGTTCTGACGTGGGGCC3’	*rev7-42 aa* truncation (rev7-42-3MYC-KANMX)
OSB120-RP	5’GTCGACCTGCAGCGTACGAAACAAAGATCCAAA AATGCTC3’	*rev7-42 aa* truncation (rev7-42-3MYC-KANMX)
OSB121-FP	5’GAGCATTTTTGGATCTTTGTTTCGTACGCTGCAG GTCGAC3’	*rev7-42 aa* truncation (rev7-42-3MYC-KANMX)
OSB61-FP	5’GGAATTC**CATATG**TCATTCACCTTGCCGCAGTTC 3’	pGBKT7_REV7-N1
OSB62-FP	5’GGAATTC**CATATG**ACCCACGTTTACAGATTTTCC 3’	pGBKT7_REV7-N2
OSB63-FP	5’GGAATTC**CATATG**TTGGAACTAGGACATAAGTTG G3’	pGBKT7_REV7-N3
OSB64-RP	5’CG**GGATCC**TTAGACTAAAGAAGTGAGTTTTATTT TAGG3’	pGBKT7_REV7-C1
OSB65-RP	5’CG**GGATCC**TTATTCTGCTTTTTCCTCCAAACTAT C3’	pGBKT7_REV7-C2
OSB66-RP	5’CG**GGATCC**TTACAATTCGATCGCATTAATAACTG C3’	pGBKT7_REV7-C3
OSB80-FP	5’CG**GGATCC**ATGTCGAAAGCTACATATAAG3’	pFAT10_ura3-G4
OSB81-RP	5’**CCC**GGT**CCCCCC**AACGACAACA**CCC**AATCAACC AATCGTAACC TTC3’	pFAT10_ura3-G4
OSB82-FP	5’**GGG**TGTTGTCGTT**GGGGGG**ACC**GGG**ATGACAC CCGGTGTGGG3’	pFAT10_ura3-G4
OSB83-RP	5’AC**ATGCAT**GCTTAGTTTTGCTGGCCGCATC3’	pFAT10_ura3-G4
OSB129-RP	5’CTCATAGCATCCAACGACAACACGCAATCAACCA ATCGTAACCTTC3’	pFAT10_ura3-G4 mutant
OSB130-FP	5’GCGTGTTGTCGTTGGATGCTATGAGATGACACC CGGTGTGGG3’	pFAT10_ura3-G4 mutant
OSB125-RP	5’GC**AAGCTT**TTAGACTAAAGAAGTGAGTTTTATTTT AGG3’	pET28_ScRev7-C1
REV7GFP-FP	GC**TCTAGA**ATGAATAGATGGGTAGAGAAG	pPROEX_ScREV7-eGFP
REV7GFP-RP	CCG**CTCGAG**GTTAATTAACCCGGGGATCCGAAAC AAAGATCCAAAAATGC	pPROEX_ScREV7-eGFP

The bold letters correspond to restrictions sites.

Table S7. Sequences of oligonucleotides used in the preparation of DNA substrates.

OSB 17 Duplex-41 bp	5’GCCGTGATCACCAATGCAGATTGACGAACCTTTGCCCACGT3’
OSB 20 Duplex-41 bp	5’ACGTGGGCAAAGGTTCGTCAATCTGCATTGGTGATCACGGC3’
OSB 41 Duplex-60 bp	5’GGGTGAACCTGCAGGTGGGCAAAGATGTCCTAGCAATGTAATCGTCAA GCTTTATGCCGT3’
OSB 42 Duplex-60 bp	5’ACGGCATAAAGCTTGACGATTACATTGCTAGGACATCTTTGCCCACCT G CAGGTTCACCC 3’
OSB28 (4G3) G4-DNA	5’AATTCT**GGG**TGTGT**GGG**TGTGT**GGG**TGTGT**GGG**TGTGG3’

OSB 92 (TP) G4-DNA	5'TGGACCAGACCTAGCAGCTAT**GGGGG**AGCT**GGGG**AAGGT**GGG**AATGTGA3'
ODN 6G3 G4-DNA	5'AATTCT**GGG**TGTGT**GGG**TGTGT**GGG**TGTGT**GGG**TGTGT**GGG**TGTGT**GGG**TGTGG3'
OSB132 (TP-G4mutant)	5'TGGACCAGACCTAGCACTATCTGCAAGTCAAGTTGACTACGTATACATA3'